UNIVERSITY OF CALIFORNIA,
IRVINE

Short-time Scale Dynamics of Marine-terminating Glaciers in Western Greenland

DISSERTATION

submitted in partial satisfaction of the requirements
for the degree of

DOCTOR OF PHILOSOPHY

in Earth System Science

by

Emily Kane

Dissertation Committee:
Professor Eric Rignot, Chair
Associate Researcher Jeremie Mouginot
Associate Professor Mathieu Morlighem

2020

TABLE OF CONTENTS

LIST OF FIGURES

ACKNOWLEDGMENTS

I would like to express the deepest appreciation to my committee chair, Professor Eric Rignot, who has been nothing but encouraging, open-minded, and supportive throughout these last 5 years. Without his guidance and persistent help this dissertation would not have been possible. I am forever thankful for the incredible graduate student experience I had in the Rignot Research Group.

I would like to thank my committee members, Professor Mathieu Morlighem and Professor Jeremie Mouginot, whose help, availability, friendship, and encouragement has been a pivotal component of this dissertation.

An exceptionally large thank you to the entire Cryosphere Group at UCI, specifically the members that accompanied me on field trips in Greenland. Romain Millan, Jeremie Mouginot, Xin Li, Mike Wood, Hongju Yu, and Virginia Brancato deserve a bright recognition as this data would not have been collected if it were not for these two great field teams.

I would also like to thank Dr. Danny Mann of UCI's Division of Teaching Excellence and Innovation (DTEI) and the rest of the staff at DTEI along with Earth System Science professors Julie Ferguson and Elizabeth Crook for sharing with me their passion for teaching and inspiring my career choice.

My parents, brother, boyfriend, and friends have helped to keep me sane throughout this degree program with constant support from near and far. I would not have completed this degree without the incredible help and encouragement of my family and friends.

Financial support was provided by the University of California, Irvine, the Jenkins Family Gradate Fellowship, and the National Aeronautics and Space Administration grants NNX17AI02G and 80NSSC18M0083, and Ocean Melting Greenland Award 1528152.

CURRICULUM VITAE

Emily Kane

EDUCATION

Doctor of Philosophy in Earth System Science — **2020**
University of California Irvine — *Irvine, CA*

Master of Science in Earth System Science — **2017**
University of California Irvine — *Irvine, CA*

Bachelor of Science in Meteorology — **2015**
Plymouth State University — *Plymouth, NH*

RESEARCH EXPERIENCE

Graduate Research Assistant, Earth System Science — **2015–2020**
University of California, Irvine — *Irvine, California*

Undergraduate Researcher, Meteorology — **2010–2011**
Plymouth State University — *Plymouth, NH*

TEACHING EXPERIENCE

Associate Faculty — **2019–2020**
Saddleback College — *Mission Viejo, CA*

Summer Instructor of Record — **2019–2020**
University of California Irvine — *Irvine, CA*

Pedagogical Fellow — **2019**
Division of Teaching Excellence and Innovation, UCI — *Irvine, CA*

Teaching Assistant — **2007–2019**
University of California Irvine — *Irvine, CA*

REFEREED JOURNAL PUBLICATIONS

Short-term dynamics of marine terminating glaciers in Torssuquak Fjord, Greenland **2020**
E. Kane, E. Rignot, M. Wood, J. Mouginot, B. Scheuchl, M. Fahnestock

Geophysical Research Letters, in preparation

Impact of calving dynamics on Kangilernata Sermia, Greenland **2020**
E. Kane, E. Rignot, J. Mouginot, R. Millan, X. Li, B. Scheuchl, M. Fahnestock

Geophysical Research Letters

Ocean Forcing Drives Glacier Retreat in Greenland **2020**
M. Wood, E. Rignot, L. An, A. Bjørk, M. van den Broeke, C. Cai, I. Fenty, **E. Kane**, D. Menemenlis, R. Millan, M. Morlighem, J. Mouginot, B. Noel, B. Scheuchl, I. Velicogna, J. Willis, H. Zhang

Science Advances (submitted)

The International Bathymetric Chart of the Arctic Ocean Version 4.0 **2020**
M. Jakobsson, L. Mayer, C. Bringensparr, C. Castro, R. Mohammad, P. Johnson, T. Ketter, D. Accettella, D. Amblas, L. An, J.E. Arndt, M. Canals, J. Casamor, N. Chauché, B.Coakley, S. Danielson, M. Demarte, M.Dickson, B. Dorschel, J. Dowdeswell, S. Dreutter, A. Fremand, D. Gallant, J. Hall, L. Hehemann, H. Hodnesdal, J. Hong, R. Ivaldi, **E. Kane**, I. Klaucke, D. Krawczyk, Y. Kristoffersen, B. Kuipers, R. Millan, G. Masetti, M. Morlighem, R. Noormets, M. Prescott, M. Rebesco, E. Rignot, I. Semiletov, A. Tate, P. Travaglini, I. Velicogna, P. Weatherall, W. Weinrebe, J. Willis, M. Wood, Y. Zarayskaya, T. Zhang, M. Zimmermann, and K. Zinglersen

Natura Scientific Data

Bathymetry of southeast Greenland from oceans melting Greenland (OMG) data **2019**
L. An, E. Rignot, N. Chauche, D.M. Holland, D. Holland, M. Jakobsson, **E. Kane**, M. Wood, I. Klaucke, M. Morlighem, I. Velicogna, W. Weinrebe, J.K. Willis

Geophysical Research Letters

CONFERENCE PRESENTATIONS

E. Kane, E. Rignot, J. Mouginot, M. Wood, M. Fahnestock (2018), Short-term velocity and variablity of west Greenland glaciers, Poster. *American Geophysical Union, Fall Meeting 2019*, San Francisco, CA.

E. Kane, E. Rignot, M. Wood, M. Fahnestock (2018), Calving and ocean impact on short-term velocity of Western Greenland glaciers, Poster. *American Geophysical Union, Fall Meeting 2018*, Washington DC.

E. Kane, E. Rignot, J. Mouginot, M. Fahnestock, (2017), Impact of calving and ocean regime on the speed of Kangilerngata Sermia, Greenland, Poster. *American Geophysical Union, Fall Meeting 2017*, New Orleans, LA, USA.

E. Kane, E. Rignot, J. Mouginot, (2017), Extension of short-term variation study of Kangilerngata Sermia, Greenland, *OSPA invited talk at American Geophysical Union, Fall Meeting 2017*, New Orleans, LA, USA.

***E. Kane**, E. Rignot, J. Mouginot, X. Li, R. Millan, M. Fahnestock, , Y. Nakayama, B. Scheuchl, (2016), Measuring short term velocity changes of Kangilerngata Sermia, west Greenland using a Gamma Portable Radar Interferometer, Poster. *American Geophysical Union, Fall Meeting 2016*, San Francisco, CA, USA.

AWARDS

- DTEI Summer Fellowship Coordinator (UCI) - 2020
- Pedagogical Fellowship (UCI) - 2019
- National Science Foundation Graduate Research Fellowship, Honorable Mention - 2017
- ***Outstanding Student Paper Award - AGU Fall Meeting 2016
- Jenkins Family Graduate Fellowship (UCI) - Fall 2015- Spring 2016
- NASA Space Grant Scholarship (PSU) - 2014-2015

ABSTRACT OF THE DISSERTATION

Short-time Scale Dynamics of Marine-terminating Glaciers in Western Greenland

By

Emily Kane

Doctor of Philosophy in Earth System Science

University of California, Irvine, 2020

Professor Eric Rignot, Chair

Iceberg calving is a major component of glacier mass ablation that is not well understood due to a lack of detailed temporal and spatial observations. For better understanding, it is critical to examine processes occurring on the time scale of calving processes, sub-daily to sub-hourly. Current satellites are not able to observe the same location at time scales small enough to measure sub-daily phenomena. This research aims to increase the temporal resolution of ice speed and elevation measurements during the calving season to allow for analysis of short-term variations that are otherwise unobserved. We measure glacier speed and surface elevation at 3-minute intervals using a portable radar interferometer at three marine-terminating glaciers in West Greenland over two summer field campaigns. We detect diurnal variations in glacier speed caused by tidal height changes that propagate far inland, the effect of which varies by glacier but are consistent with simple models where basal stress is tidally modulated. We find no speed up from ice shedding off the calving face or the detachment of floating ice blocks, as expected. We detect a 30% speedup within a few hundred meters of the ice front that persists for days when calving removes full thickness grounded ice blocks. Within one ice thickness from the calving front, we detect strain rates 2 to 3 times larger than observable from satellite data, which has implications for studying iceberg calving as a fracturing process, in particular to select an appropriate value of the threshold tensile stress necessary for ice cliff failure.

Chapter 1

Introduction

1.1 Background

The Greenland Ice Sheet has been losing mass for decades at an increasing rate and is contributing significantly to sea level rise (Mouginot et al., 2019). Marine terminating glaciers control 50-60% of glacial mass loss (Rignot et al., 2008; Mouginot et al., 2019), with the other 40-50% controlled by surface melt processes. Glacier mass losses result from glacier speed up, increased production of icebergs, enhanced undercutting of ice by warm ocean waters, and increased surface melt (Motyka et al., 2003; Rignot et al., 2016). Iceberg calving is a major component of the mass loss at frontal margins (Benn et al., 2007) and the least well understood and modeled component (DeConto and Pollard, 2016). It is important to understand the physical processes driving calving events to better quantify Greenland's potential contribution to sea level rise.

Marine-terminating glaciers are those that flow downstream and end in the ocean. Ice at the glacier front can detach and float away as an iceberg during as an act of calving. Calving can be caused by longitudinal extension of the glacier ice, melt undercutting from the ocean

waters, or buoyancy (Benn et al., 2007). Calving occurs when the tensile stress of the ice reaches a certain threshold. Understanding the dynamics of marine-terminating glaciers and how they calve is critical to ice sheet models.

To improve our understanding of iceberg calving and its impact on ice dynamics, it is critical to collect data at the same temporal and spatial scales as that of the physical processes that control these calving events, which means minutes to hours for periods of several days (Cassotto et al., 2015) and with sufficient spatial resolution to observe crack and rift formation. Such combination of high temporal and spatial resolution is not currently available from satellites.

Spaceborne interferometric radar (InSAR) has been used to measure ice velocity at the continental scale on an annual to monthly basis, with a temporal resolution defined by the repeat pass cycle of the satellite (Riesen et al., 2011), which is weeks for most systems, except for the 1-day repeat from the Agenzia Spaziale Italiana's Cosmo SkyMed constellation (Covello et al., 2010; Milillo et al., 2017). Current satellites do not have short-enough repeat cycles to resolve the connection between glacier speedup and processes such as tidal forcing or calving of icebergs on sub-daily time scales.

Previous remote sensing studies show Greenland glaciers display weekly to seasonal variations in ice speed. Data acquired at Helheim Glacier with an 11-day repeat cycle using the German Aerospace Center's (DLR) TerraSAR-X showed that ice velocity peaks in the summer months, but daily details within the summer season are few (Joughin et al., 2012). Hourly and daily variations in ice velocity measured using Ground Positioning System (GPS) (Sugiyama and Hilmar Gudmundsson, 2004; Amundson et al., 2008; Nettles et al., 2008) have shed light on glacier dynamics at sub-daily temporal scales, but these in-situ methods require a network of observations that is challenging to maintain over a large glacier. The difficulty of maintaining a GPS network near or at a calving front further limits their utility at calving margins.

The lack of temporal resolution in these time series leaves much to be determined about the large variability in the data sets. Many processes shown to cause variability in tidewater glacier velocities are not captured by satellites with bi-monthly repeat acquisitions, such as tidal cycle, calving events, melange concentration, or subglacial variability.

The Gamma Portable Radar Interferometer (GPRI) (Fig. 1.1) has been employed to fill the gap between weekly measurements at the continental scale by satellites and nearly-continuous data at discrete locations from GPS. It provides high temporal resolution, typically minutes, at a high spatial resolution, typically a few 10's of meters, over many square kilometers of glacier area. Using data collected at sub-daily timescales, researchers have been able to link fluctuations in glacier speed with the tidal cycle (Voytenko et al., 2015; Cassotto et al., 2015; Holland et al., 2016; Xie et al., 2018), melt water production (Shepherd et al., 2009; McGrath et al., 2011), melange concentration near the ice front (Cassotto et al., 2015; Xie et al., 2019), and large calving events (Cassotto et al., 2018; Holland et al., 2016). However, much uncertainty remains in our understanding of the relationship between calving events, glacier speed, ice thickness, and bathymetry. In particular, it is not clear why some calving events produce a change in speed while others do not.

For these studies, calving is defined as removal of a full-thickness piece of ice from the glacier ice front. These events produce visible gravity waves in the fjord and a change in ice front position detectable in the GPRI MLI imagery. Smaller events, defined here as shedding, produce visible gravity waves in the fjord but result in no change in ice front position. These events do not remove full-thickness ice from the ice front.

Ocean forcing plays a large but not well understood role in ice loss acceleration. Ocean profile data obtained via Conductivity, Temperature and Depth sensor (CTD) casts allow for melt water rate calculations and water mass categorization that will provide important insight to the forcing of the ocean on the calving front. Improving our understanding of the physical mechanisms that influence calving events has the potential to improve our total

understanding of Greenland ice sheet mass loss, to improve the current ice sheet modeling techniques and reduce uncertainties in projecting future sea level changes.

The fjords where Greenland's glaciers terminate consist of cold, fresh polar water atop warmer (2-5C), saltier Atlantic water (AW) (Straneo et al., 2010) (Fig. 1.2). Warm AW mixing with the rising fresh subglacial discharge drives high submarine melting which causes undercutting of the calving fronts (Rignot et al., 2010). AW is pushed by winds into fjords that are deep enough (> 300 m) to access the glaciers (Straneo et al., 2010). By combining ADCP and CTD across the glaciers (with a sample of about every 300 m or one ice thickness), estimations can be made for the heat, salt, and mass budget of the ocean water.

This work aims to investigate the dynamics of marine terminating glaciers on sub-hourly timescales and report on findings gleamed from two multi-week field campaigns to Western Greenland in 2016 and 2018. Here, we propose to gain insights into short-term glacial processes by observing glaciers with a time scale of a few minutes and integrate this data into currently available velocity time series. Using radar interferometry techniques we investigate the dynamics of the tidewater glaciers sub-hourly. This work will use GPRI data collected during the time of highest calving activity, July, with the goal of understanding the gaps in existing satellite data in order to better plan future missions.

1.2 Techniques

1.2.1 InSAR and satellite data

A Synthetic Aperture Radar (SAR) is a spaceborne or airborne sidelooking radar that can generate very high resolution remote sensing imagery. Pulses of electromagnetic energy are reflected off of the Earth's surface back to the satellite or aircraft. Signal processing uses

the intensity and phase of the radar images to create a high resolution image of the terrain below (Robert Massom, Dan Lubin, 2006). The intensity image is relative to the amplitude of the radar signal (amplitude of the electromagnetic wave), and the phase is relative to the phase of the signal. Different look angles can be used to recover height information, allowing for creation of Digital Elevation Models (DEMs).

Using the measured differences in phase of the return signal between two SAR acquisitions, slight changes on Earth's surface can be detected, including surface elevation and glacier flow. This process, Synthetic Aperture Radar Interferometry (InSAR), has revolutionized our ability to track the motion of glaciers at very high resolutions of mm to cm for surface displacement and meters for surface elevation (Robert Massom, Dan Lubin, 2006). We use InSAR to track the short time scale changes measured by a GPRI.

Remote sensing derived velocity maps have been produced annually for the entire Greenland Ice Sheet since 1972 (Mouginot et al., 2017; Rignot and Mouginot, 2012). Using a combination of optical and synthetic aperture radar (SAR) missions, large scale velocity processing has become common practice. Mosaics of all available data provide an unparalleled understanding of the ice sheet's history (Mouginot et al., 2017), with a temporal resolution limited to the length of time between repeat passes to the same location (Riesen et al., 2011).

The dynamics and structure of tidewater glaciers will be reconstructed using all available satellite products to create a time series of speed, ice front position, and surface elevation back to 1980. The synthesis of velocity data beginning in 1984 from Landsat-4, 5, 7, 8, ERS-1,2, RADARSAT-1,2, ALOS/PALSAR, ENVISAT/ASA, TerraSAR-X, and Sentinel-1a, b allow for the most complete and dense history of ice velocities using radar interferometry and feature tracking. This available time series shows sub-yearly velocity variations with seasonal velocity patterns visible from 2013 onward due to increased temporal resolution from Sentinel-1a, b and Landsat-8.

Historical ice front positions are be determined using Landsat-8, Sentinel-1ab, Sentinel-2, and MODIS where available. Surface elevation evolution is extracted from IceSAT1-2, TanDEM-X and WorldView. With historical knowledge of ice velocities, ice front position, ice surface elevation, and high resolution bathymetry from NASA's Oceans Melting Greenland (OMG) 2016 (2016) we can begin to assess the variability seen in these records. The history of the glacier's speed and height changes are essential to create a context for understanding the GPRI derived products.

We processed other SAR data (TerraSar-X) over the time period of investigation to compare with GPRI measurements. These satellites have 11 day repeat cycle. We also utilize the suite of processed satellite data for each glacier of study (Mouginot et al., 2017, 2019) to compare velocity values and coverage across the glacier fronts. The results of these comparison determine what information is lost or may be recovered from these longer-term resolution data about calving events. We also access World View imagery and associated DEMs processed as part of the Greenland Mapping Project (GIMP-3) for comparison with our GPRI-derived DEMs (Porter et al., 2018; Howat et al., 2014).

Long term weekly time series will be analyzed alongside the sub-hourly data to determine how the data sets can be used together. This is instrumental in determining what best temporal resolution SAR systems should achieve to observe calving dynamics.

1.2.2 GPRI

We investigate the short term velocity and height variations by comparing the GPRI time series to tide gauge, ice front position, calving events, precipitation, and weather data. The resolution of the GPRI data can capture the influence of tides, precipitation, melange presence and concentration, calving events, and changes in sub-glacial hydrology on glacier speed and surface height.

GPRIs have a number of advantages for remote sensing of ground deformation including: mm-scale accuracy, spatial resolution, and relative insensitivity to clouds compared to LiDAR (laser scanners) Werner et al. (2008); Voytenko et al. (2015). The GPRI also has the ability to conduct frequent measurements (to observe fast, minute-scale, displacement variations and to reduce atmospheric effects) at a variety of imaging geometries with flexible survey timing compared to aircraft or satellite-based radars

Long term weekly time series will be analyzed alongside the sub-hourly data to determine how the data sets can be used together. With a goal of understanding processes that lead to changes in dynamics of tidewater glaciers we will use the GPRI data to fill in the missing pieces of the satellite time series. The comparison will determine what information is lost or may be recovered from these longer-term resolution data. Analysis of ice front changes and the relation to bed topography will be crucial in understanding the past of each tidewater glacier.

GPRI is a real-aperture interferometric radar operating at 17.2 GHz, with a range of 16 km, one transmitting antenna and two receiving antennas (Fig. 1.3) that scan in azimuth by rotating around a vertical axis, acquiring images range line by range line (Werner et al., 2008) (Fig. 1.4). Phase noise in the line of sight is limited by turbulent water vapor mixing (Riesen et al., 2011). The GPRI operated over a 90 degree arc scanned during a 20 second data acquisition. Azimuth resolution varies from 28 m at 3.5 km from the ice front to 40 m upstream in the far range of our data. The baseline length is 25 cm. Data are collected at 3 minute intervals except when the antennas were removed due to high wind and/or heavy rain.

We generate a time series of 3-minute radar interferograms from GPRI single-look complex images using the Gamma Remote Sensing software package (Werner et al., 2008). We multi-look the GPRI data using 5 range looks and smooth the interferograms using an adaptive filter (Goldstein et al., 1988) with a filtering window of 64 range/azimuth cells with an

exponent of non-linear filtering of 1 to maximize unwrapping without introducing phase jumps. We unwrap the interferometric phase from the filtered interferograms as explained in (Goldstein et al., 1988).

The phase difference, ϕ, between successive images determines the line-of-sight (LOS) displacement:

$$\delta_{los} = \frac{\lambda\phi}{4\pi}$$

, where λ is the wavelength (17.4 mm) (Goldstein et al., 1988; Kwok and Fahnestock, 1996). The displacements are converted into LOS velocities as:

$$V_{los} = \frac{\delta_{los}}{\delta t}$$

where δt is the time interval between acquisitions, which for this data is 3 minutes. V_{los} can then be converted into horizontal speed, V, as:

$$V = \frac{V_{los}}{cos(\alpha)cos(\zeta)sin(\theta) - sin(\alpha)cos(\theta)}$$

where α is the surface slope from the GPRI-derived DEM, ζ is the angle between the TerraSAR-X derived ice flow direction and GPRI look direction, and θ is the radar incidence angle (Kwok and Fahnestock, 1996). We assume no variation in flow direction during the period of observation.

The 3-min displacement results are affected by turbulent atmospheric water vapor (Voytenko et al., 2015). To minimize noise, we stack the interferograms in time (Werner et al., 2008). We performed an analysis to determine optimal stack lengths (Figure 1.5). We found atmospheric noise ranges from 250 to 1 m/yr based on stacking widows of 3 minutes to 6 hours (Fig. 1.5). We used 30-minute stacked data to reduce errors to around 40 m/yr while preserving the high-resolution signal needed for our study.

The dual receiving antennas on the GPRI allow for topographic interferograms between two single-look complex images acquired simultaneously. The interferograms are unwrapped and converted from phase into surface elevation (Goldstein et al., 1988) using ground control points on land extracted from a World View ArcticDEM (Porter et al., 2018). We generate a time series of GPRI DEMs using data averaged over 30-minute periods.

We use the time series of GPRI derived-elevation above mean sea level to calculate the height of the ice surface above flotation. We assume that the glacier is grounded when its ice surface elevation is above hydrostatic equilibrium. The height above flotation,

$$h_f = h - \frac{H((\rho_w - \rho_i)}{\rho_w)}$$

where ρ_i is the column-averaged density of ice, 910 kg/m^3, and ρ_w is the density of seawater, 1027 kg/m^3, and h is the time series of 30-min average GPRI DEMs, and the ice thickness, H, is h minus the depth of the sea floor (variables shown in Fig. 1.7). The density of seawater is the column-averaged density based on Conductivity, Temperature, and Depth (CTD) measurements taken 1 km from the glacier front. The uncertainty in height above flotation combines the uncertainty in h (1-2 m) (Fig. 1.6), bathymetry (1-2 m), and ice and water densities (10%), for a combined 4 m error.

A comparison by (Choi et al., 2018) of different calving laws concluded that the calving law based on the von Mises (VM) stress (Morlighem et al., 2016) produces the best fit with observations. In that approach, calving occurs when the tensile stress exceeds a threshold σ_{max}. We calculate the effective tensile strain rate, $\dot{\varepsilon_e}$, as:

$$\dot{\varepsilon_e}^2 = \frac{1}{2}\left((max(0, \dot{\varepsilon_1})^2 + (max(0, \dot{\varepsilon_2})^2)\right)$$

where $\dot{\varepsilon_1}$ and $\dot{\varepsilon_2}$ are the two eigenvectors of the 2-D strain rate tensor derived from the GPRI-derived velocity (Morlighem et al., 2016). We then convert strain rate to stresses,

σ_{max}, across the ice front as:

$$\sigma_{max} = \sqrt{3} B \dot{\varepsilon_e}^{1/3}$$

Here, we use a deformation constant (B) of 324 kPa/yr$^{1/3}$, the suggested value for ice at -5°C, with an uncertainty of 25% (Cuffey and Paterson, 2010).

1.2.3 Limitations

The GPRI is a powerful instrument that acquires data every 3 minutes through dark, clouds, and light weather. During heavy rain and heavy wind however, the antennas must be removed to preserve the integrity of the GPRI's vertical stand. For this reason, along with the necessity of electricity to run the GPRI, a human crew is needed to operate the instrument when deployed in the field.

While GPRI is useful to examine processes taking place at high temporal scale, it can only be deployed on a few glaciers over limited periods of time without protection from wind and weathering and without securing of long-term energy supply. The GPRI can only observe up to 16 km from the base. Both field campaigns discussed here show increased noise starting at 8 km in azimuth. During the 2016 field campaign a faulty wire caused the power of the instrument to decrease dramatically, causing additional difficulties when processing.

Synthetic aperture instruments require good coherence/correlation over the time of the scan. Loss of coherence will occur if there are large displacements within the area of interest. The GPRI has a longer scan time, meaning decorrelation issues may arise during acquisitions when monitoring fast-moving (20 m/d or greater) glaciers Voytenko et al. (2015). Decorrelation can also be an issue over longer (hour-scale or longer) periods. Unwrapping becomes difficult at these longer time periods due to decorrelation of the glacier surface when the motion between acquisitions is larger than multiple radar wavelengths.

GPRI field campaigns require significant preparation. The GPRI must be set up on stable ground with a clear view of the glacier front of interest. The elevation of the instrument should be high enough to avoid shadowing on the glacier surface. The location GPRI should be such that the majority of the ice motion is along the radar line-of-sight (LOS) and the viewing arc include stationary rock to use as ground control points.

1.3 Field Methods

1.3.1 GPRI

Two multi-week field campaigns made use of GPRI measurements along marine terminating ice fronts in Western Greenland. Both campaigns were aimed at observing the short-term dynamics of ice fronts in July when iceberg calving is at its peak.

A group of four researchers accompanied the GPRI on a field campaign to Kangilernata Sermia in northen Disko Bay (Fig. 1.6) from 04 July -19 July 2016. This successful research trip collected continuous GPRI data every 3 minutes with few exceptions for high wind. The GPRI was located 3.5 km from the center of the ice at an elevation of 168 m elevation with no movement of the instrument base. The GPRI was powered by batteries and a generator alternating in 3-5 hour increments (Fig. 1.3). When powered directly by the generator, the batteries were charging.

A second field campaign from 03 July -14 July 2018 utilized a GPRI at Torsukataq Fjord in Northern Disko Bay (Fig. 1.6) acquiring data of both Seremeq Kujalleq and Seremeq Avannarleq. A group of four researchers accompanied the GPRI for 15 days alongside Kujalleq Glacier. The GPRI was situated at 113 m above sea level for the entire field campaign, 3,400 m from the center of Kujalleq's ice front and 7,700 m from the ice front

of Avannarleq. The same power system was used as at Kangilernata in 2016 with both a generator and batteries to keep the GPRI running at all times. Few multi-hour breaks required removal of the GPRI antennas due to high wind and/or heavy rain.

1.3.2 CTD and ocean data

This research has included CTD data collection across the Kangilernata Sermia ice front in July 2016. We were able to complete 7 full CTD transects of 12 casts each, locations shown in Figure 3.6. Data was collected at different times and on different days to sample daily to sub daily variability and reduce uncertainties. CTD data includes temperature, salinity, and dissolved oxygen, which can be used for melt rate estimation of glaciers wide enough to assume geostrophic flow (Jenkins and Jacobs, 2008).

1.4 Research objectives

My main dissertation objectives are to better understand the short term dynamics of marine-terminating glaciers by addressing the following questions:

1. What is the significance of short-term glacier variability that cannot be measured by current satellites? 2. What drives the variability visible in satellite data? Can this be explained with TRI measurements? 3. How does the rate of calving compare with the deviation from hydrostatic equilibrium?

These questions are addressed using multi-week GPRI data sets of ice velocity and elevation at 3 marine-terminating glaciers in Greenland combined with a data set of all available satellite data from (Mouginot et al., 2017, 2019).

Figure 1.1: GPRI operational at Torsukatqk Fjord in July 2018. Kujalleq glacier seen in the background.

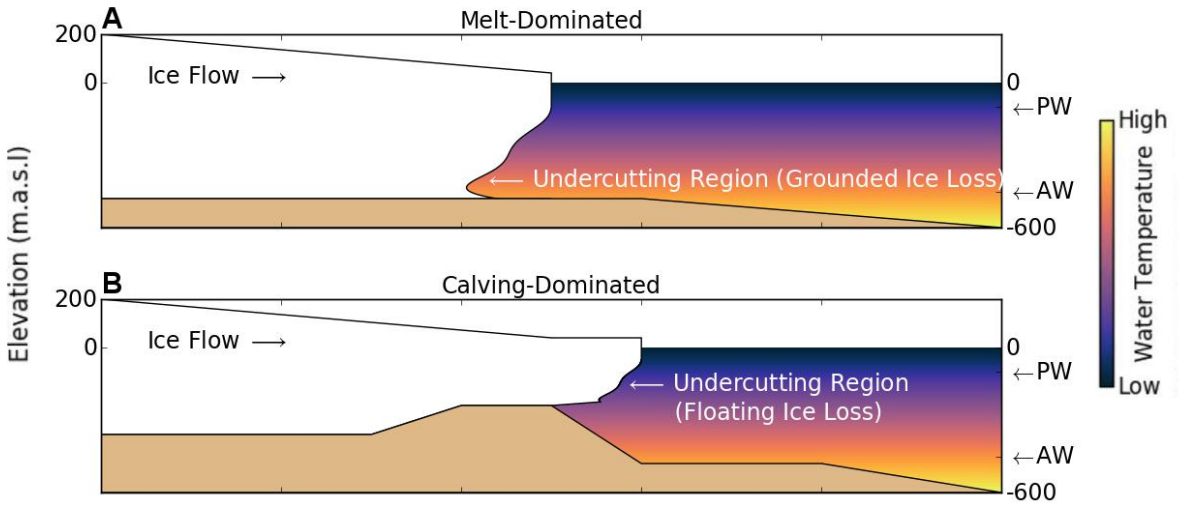

Figure 1.2: Ocean temperature profiles along marine-terminating glaciers in Greenland. Dense, salty Atlantic Water (denoted AW) beneath fresh Polar Water (denoted PW) at the surface. Adopted from Wooed et al. 2020 (in review).

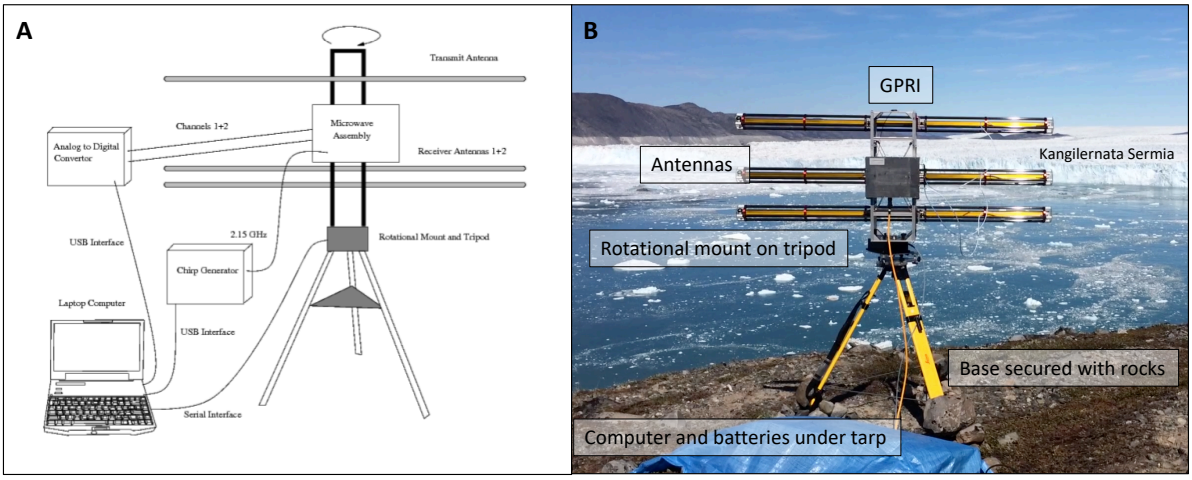

Figure 1.3: GPRI Hardware components (left) from Werner et al., 2008 and a photo of GPRI deployed at Kangilernata Sermia (right) in July 2016.

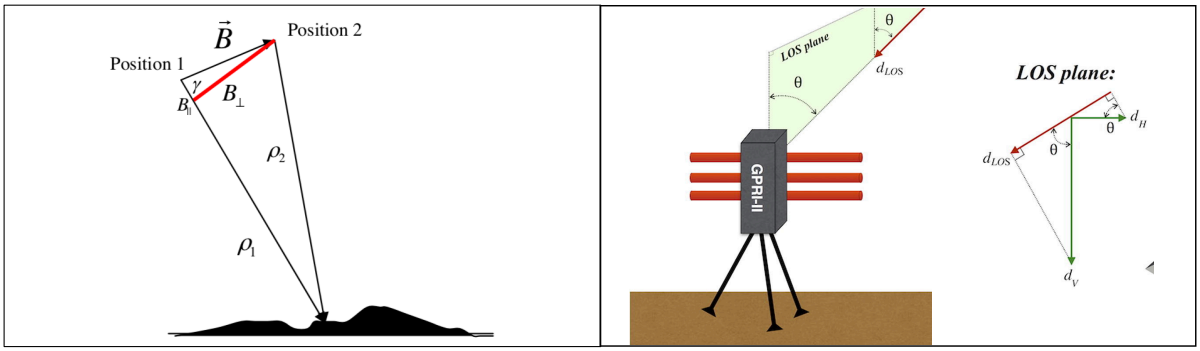

Figure 1.4: The basic geometry for interferometric data acquisition (left) adopted from Werner et al. 2008 showing the baseline B with parallel and perpendicular components and the slant range vectors 1 and 2. Illustration of GPRI geometery (right) adopted from Zhang et al., 2018, showing GPRI set up and LOS geometeries of data acquisition. dLOS, dV, dH, are ice displacements in the LOS, vertical, and horizontal directions.

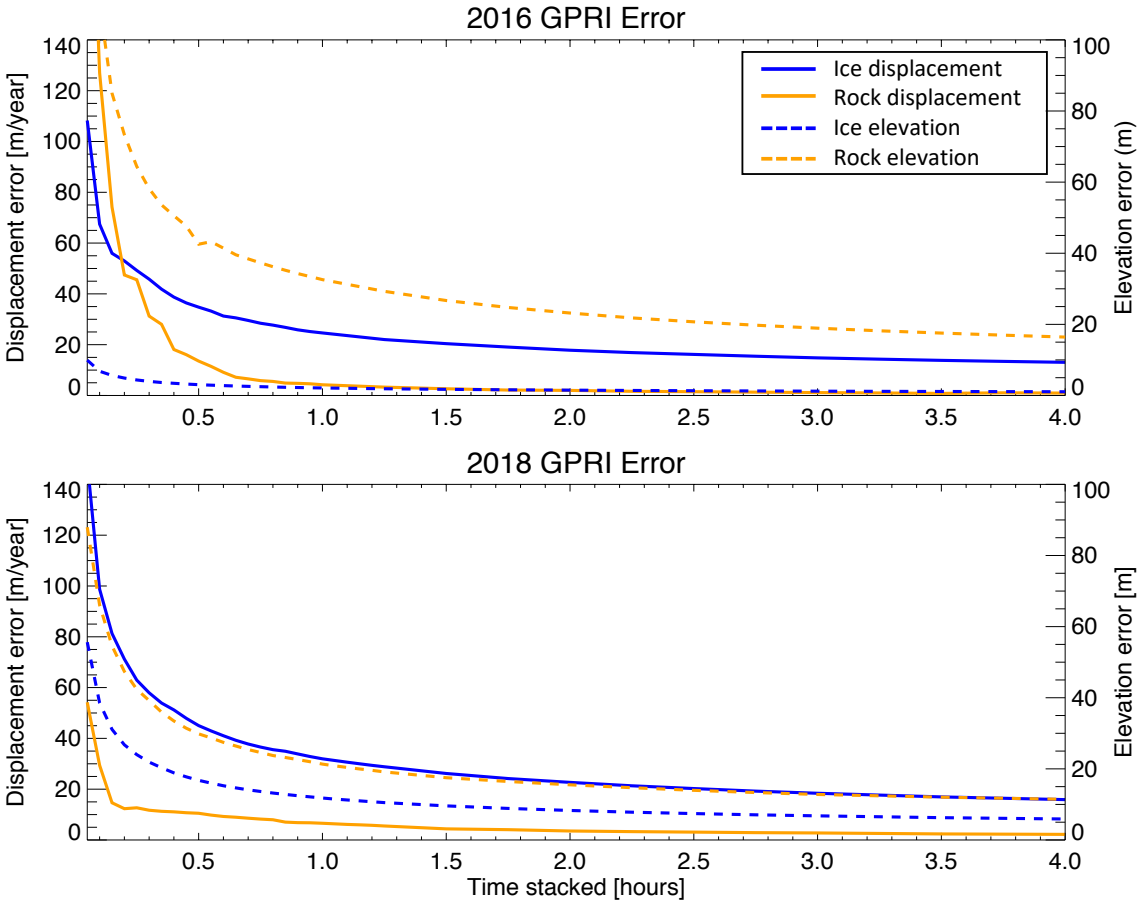

Figure 1.5: Noise of GPRI derived displacement (solid line) and elevation (dashed line) for the 2016 (top) and 2018 (bottom) field campaigns with time stacked.

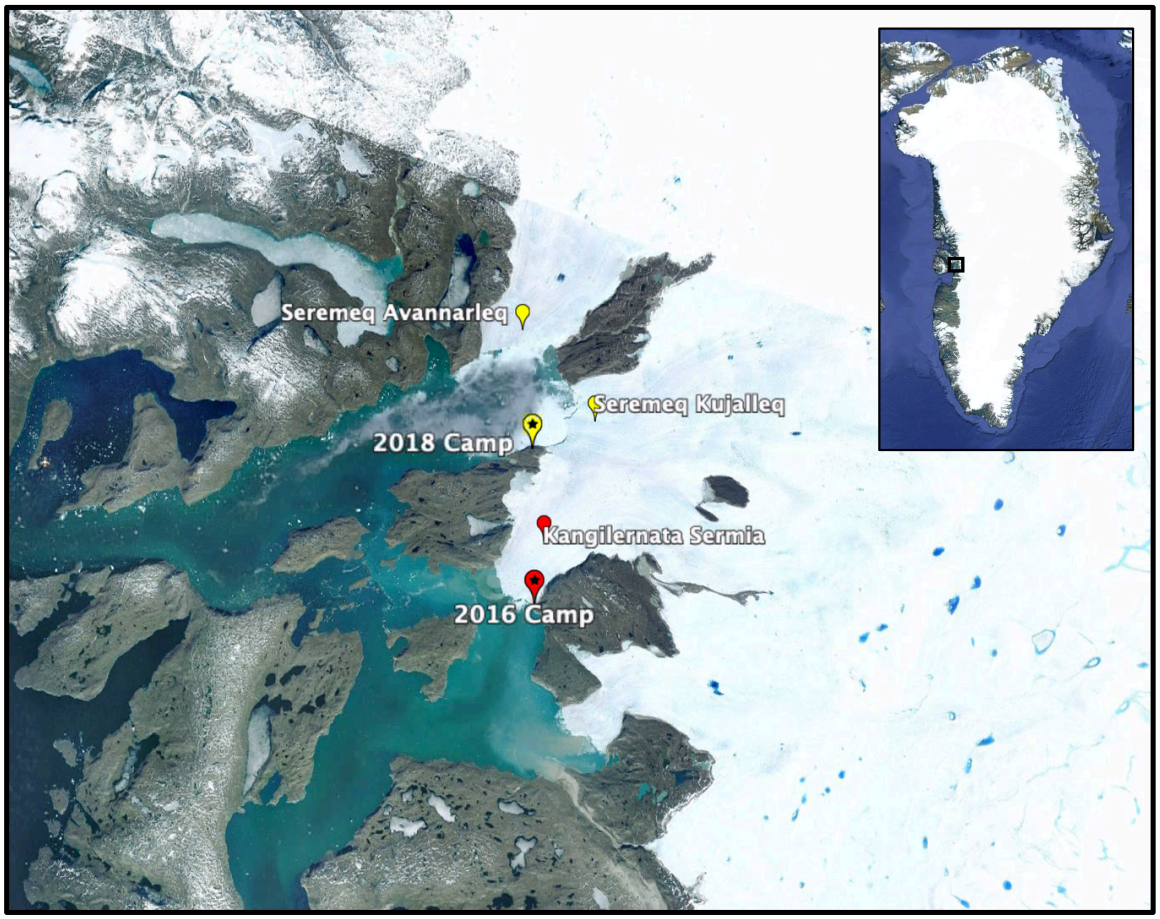

Figure 1.6: Map of northern Disko Bay, Greenland. 2016 field site in red, 2018 field site in yellow.

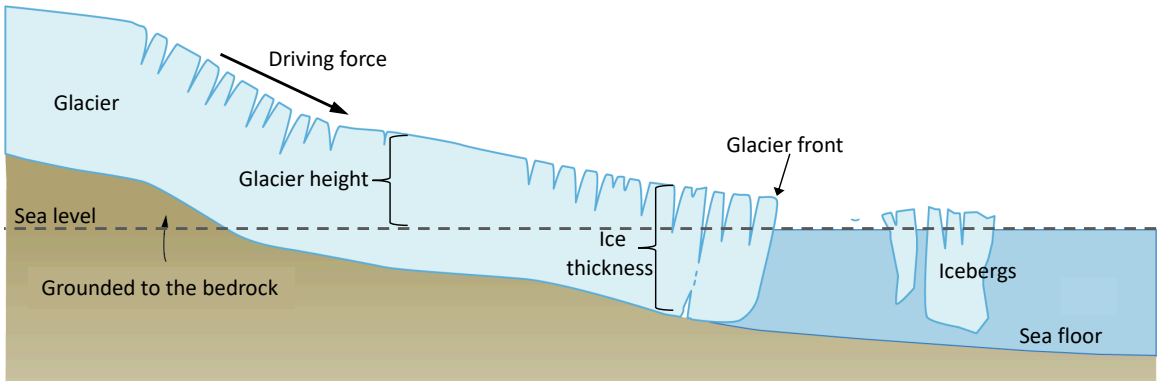

Figure 1.7: Labeled diagram of a marine terminating glacier adapted from (http://www.antarcticglaciers.org/).

Chapter 2

Impact of calving dynamics on Kangilernata Sermia, Greenland

2.1 Introduction

Kangilernata Sermia is a 3.5-km wide glacier located in north Disko Bay, Greenland. The glacier was stable on a sill 150 m below sea level from 1964 to 2004, before retreating by 3 km in 2005-2010 as the glacier detached from the sill in response to warmer ocean waters, and remained relatively stable in waters 350 m deep after 2010 (Rignot et al., 2016). Inland of the ice front, the bed elevation is 200-450m below sea level for another 30 km (Fig. 2.1A) (Rignot et al., 2016). Ice front undercutting by warm ocean waters is estimated to have increased from 1.5 m/d (meters per day) in the 1990s to 2.6 m/d in 2005-2010 (Rignot et al., 2016). For comparison, the advection of ice at the front increased from 2.2 m/d prior to 2004 to 6.5 m/d in 2012 (Rignot et al., 2016), which, combined with knowledge of ice front position retreat, has revealed that iceberg calving is a dominant component of glacier mass loss.

Here, we use GPRI to document short time scale changes in glacier speed and elevation at a high spatial and temporal resolutions for a period of two weeks, early in the summer season when most calving events take place. We evaluate the effect of tidal variations and iceberg calving on the glacier speed as a function of size, location, and characteristics of the calving events. We compare the results with surface melt production and tidal forcing. We conclude on the importance of calving events on the glacier dynamics and on the insights gained from the short-time scale observations of Greenland glaciers.

2.2 Materials and Methods

2.2.1 Satellite data and bathymetry

We assemble satellite-derived velocity measurements of Kangilernata Sermia from 1984 to present using Landsat-4,5,7,8, ERS-1,2, RADARSAT-1,2, ALOS/PALSAR, ENVISAT/ASAR, Sentinel-1a,b, and TerraSAR-X (Mouginot et al., 2017). The temporal resolution of the data depends on the native repeat cycles of these satellites, which is 16 days for Landsat, 35 days for ERS-1/2, 24 days for RADARSAT-1/2, 44 days for ALOS PALSAR, 35 days for Envisat/ASAR, 6 to 12 days for Sentinel-1a/b, and 11 days for TerraSAR-X. We extract velocity values along the 2016 front of Kangilernata Sermia (Fig. 2.1).

Fjord bathymetry was mapped with multibeam echo sounding (MBES) in year 2012 to constrain bed elevation to within 1 m (Rignot et al., 2015). Combined with a time series of 30-minute average, GPRI-derived Digital Elevation Model (DEM) of the ice surface with a precision of 1 m, we have excellent constraints on ice thickness ($\pm$1-2 m). Because the glacier re-advanced in 2012-2016, the 2012 bathymetry extends about 500 m inland of the 2016 ice front position, i.e. providing quality bed elevation data beneath the ice (Fig. 2.1A).

2.2.2 GPRI Surface Velocity and Elevation

We deployed a GPRI-II for two weeks in July 2016 on the south side of Kangilernata Sermia (Fig 1.3B), at 168 m elevation, 3.5 km from the center of the ice front (Fig. 2.1 and 2.2) collecting displacement and elevation data every 3 minutes.

Between day of year (DOY) 191 and 203 of the campaign, the intensity of the GPRI signal dropped by 3 dB as a result of a weak cable connector. The increase in system noise makes it more difficult to unwrap the phase. We alleviate this issue by unwrapping the phase by blocks and reconnecting the unwrapped blocks manually after estimating their relative phase offsets. Upstream of the ice front, our low grazing illumination angle placed some sections of the ice surface in the shadow of the radar illumination, yielding no signal.

2.2.3 Tracking Calving Events

The multi-looked radar backscatter intensity (MLI) data help geolocate the ice front at each acquisition and track the motion of iceberg debris floating at the sea surface with time. The high resolution of these acquisitions makes it possible to provide a timetable of iceberg calving and ice shedding events throughout the survey. For this study, we classify calving events as breakup of ice blocks that produce a detectable retreat of the ice front (5 m posting) and generate strong gravity waves in the fjord waters that stir the ocean waters for tens of minutes. In contrast, we refer to shedding events as breakup of ice blocks that do not produce a change in ice front position and generate gravity waves of much less magnitude. Calving events correspond to full thickness ice breakup. Shedding events do not correspond to full ice thickness breakup but to ice slabs or blocks falling off the ice face. In addition, the MLI imagery reveals the location of plumes of subglacial discharge as they disturb the ocean surface. Iceberg motion retrieved from time series of MLI images also provides information about the horizontal circulation of ocean waters in the fjord.

2.2.4 Tidal Measurements

We installed a HOBO U20 Water Level Logger (Fig. 2.3) for 10 days to collect water pressure measurements and allow for tidal height calculations. The tide gauge measured pressure below the water line at our harbor site, about 5 km away from the ice front. Data collection ended before the end of the campaign due to instrument failure.

2.2.5 CTD Measurements

Transects of CTD casts were taken by zodiac boat using 2 Minos-X profilers from AML Oceanographic (Fig 2.4). These profilers measured depth, pressure, temperature, conductivity, and dissolved oxygen. The casts were taken by hand off the side of a zodiac boat and transmitted wirelessly or via hard-wire to field computers for data analysis.

2.3 Results

2.3.1 Velocity analysis

During the GPRI survey, the 3.5-km wide Kangilernata Sermia moved at an average speed of 1,600 m/yr at the ice front (Fig. 2.1B). Two regions of fast flow are found near the location of meltwater plumes: one along the southern 1.2 km of the ice front with ice speeds in excess of 2,400 m/yr; another located in the deepest section of the fjord (350m depth) with a speed of 2,200 m/yr.

We compare the GPRI-derived velocity data with historical satellite velocity measurements at the center of the glacier, 215 m upstream from the ice front, where both satellite and GPRI data are available (Fig. 2.3A). The speed of 800 m/yr in 1976 did not change until

the early 2000s, except on occasions (1994, 2006) (Mouginot et al., 2019). In 2005, the glacier slowed before starting to retreat and speed up until 2012 when the glacier stabilized to a new bed position (Fig. 2.1D). Peak speed exceeded 2,000 m/yr in 2010-2012, followed by a slow down to 1,500 m/yr. Ice speed exhibited a seasonal variability of 20-25% during 2004-2018 (Fig. 2.3B). Yearly minima of 1,100 m/yr occur in fall and yearly maxima reach 1,900 m/yr in spring.

The GPRI-derived ice speed agrees with the satellite data from TerraSAR-X data (Fig. 2.3A-B, 2.4), which provides confidence in the measurements. In addition, the GPRI data reveal that the glacier experiences diurnal to sub-diurnal velocity variations of ±200 m/yr. Maximum speeds occur around mid-day at 2,100 m/yr and minimum speeds occur in early morning at 1,570 m/yr. Superimposed on that diurnal variation, we observe a lower frequency modulation in speed over a period of several days (Fig. 2.3C). The modulation in speed is more apparent when compared with tidal forcing. The survey started on DOY 187 during spring tides before transitioning to neap tides on DOY 194 (Fig. 2.3C). We find a correlation of 0.71 between tidal pressure and GPRI-derived ice speed with a one hour delay during spring tides (DOY 188-191) and a correlation of 0.63 and the same delay with during neap tides (DOY 193-196). During the transition from spring to neap tides, the correlation drops to 0.19. The positive correlation between tidal pressure and speed decreases inland from 0.7 within 300 m of the ice front to 0.3 about 1 km from the ice front.

Following Gudmundsson (2007), we model the glacier speed as a function of tidal pressure measured directly from the tide gauge on site, δP, using a Weertman's sliding law (Cuffey and Paterson, 2010). Using a sliding ratio, r, of 25, and a sliding speed of u_b, the total speed, u, is

$$u = (1/r + 1)u_b$$

$$u_b = C\tau_b^m$$

where C = 12x10^{-5} m/d/kPa^{-m}, the sliding exponent m = 3, and τ_b is the basal drag. Basal drag varies around a mean value modulated by tidal pressure,

$$\tau_b = \bar{\tau}_b + K\delta P$$

where the local stress ratio K is chosen to be 0.2. We calculate $\bar{\tau}_b$ =35 kPa based on the mean glacier speed over the entire period, and allow a quadratic excursion of ±9kPa in $\bar{\tau}_b$ during the survey period to best fit the residuals in mean speed. The value of K is close to that used by (Gudmundsson, 2007). We varied the sliding ration r to optimize the model fit. Despite the model simplicity, we obtain a good fit with the data, except perhaps for the brief period between DOY 193 and 195.

Daily averaged runoff values from the RACMO2.3 model (Noël et al., 2015) for the Kangilernata Sermia basin vary from 0.026 to 0.048 kg/m^2/d over the study period (Fig. 2.3E). We find no correlation between daily runoff and daily-averaged ice velocity using the modeled data. At the 95% confidence interval, the squared Pearson correlation coefficient R^2 ranges from 0.045 (P=0.18) at the ice front to 0.064 (P=0.22) about 1 km inland. We conclude that daily averaged runoff is not a viable descriptor of the variations in velocity over the two-week period of our survey. No rain event was recorded during the survey.

2.3.2 Calving event analysis

The largest calving event occurred on 12 July 2016 (DOY 194). The ice block began to detach from the ice front at 15:08 UTC and took 9 minutes to break off completely. As ice detached from the front, the block split into two pieces that moved away from the ice front within minutes (Movie S1). A 1-km long piece of ice calved from an area near floatation (Fig. 2.5A) followed by an increase in speed from 1750 m/yr to 2,400 m/yr, or 37% (Fig. 2.5E). The speed up is comparatively smaller in magnitude and does not propagate far upstream.

The calving event occurred when the tide was receding. The speed decreased slightly after reaching a peak following the calving event but persisted for the rest of the survey at about 30% above its initial value. The ice block that detached was 650 m long by 105 m wide at its largest. Most of the block was near floatation prior to detachment, but the southernmost portion, about 8,900±2,800 m^2 in area, was grounded before the calving event. We estimate the volume of the detached grounded ice block to be 3.4x10^6 m^3.

The second largest calving event occurred at 19:31 UTC on 17 July 2016 (DOY 199). This calving event detached a smaller piece of ice about 400 m long by 65 m wide from roughly the same region (Fig. 2.5B). We observed no change in speed (Fig. 2.5F). We estimate that the ice block removed an area of only 5,300±2,100 m^2 of grounded ice and an ice volume of 1.8x10^6 m^3 of grounded ice. During the rest of the survey, we witnessed many other detachments, but with no detectable impact on glacier speed (Fig. 2.3C). In all cases, we note that the change in speed does not propagate far inland, i.e. only about one ice thickness or less. In contrast, the changes in ocean tide alter the entire glacier width and propagate beyond the range of the GPRI (Fig. 2.6).

2.3.3 Strain rate analysis

The effective strain rate derived from GPRI is high along a narrow band about 300 m wide, or one ice thickness, along the ice front, with values up to 4/yr versus 0.5 to 1/yr immediately upstream (Fig. 2.1C). Such values of the strain rate are exceptionally high. The strain rates peak within 50 to 80 m from the ice front. We detect a peak strain rate of 4.5/yr along the eastern flank versus 2.5/yr along the western flank. Such high strain rates are not measurable from the TerraSAR-X-derived velocity (Fig. 2.1F) because speckle tracking is limited to areas at least a few hundred meters from the ice front due to spatial averaging (Fig. 2.1D and 27). We employed speckle tracking with smaller-sized windows, from the

nominal 128 x 96 pixels window (about 212 m x 216 m in size) that insures no data gap to a 32 x 24 pixels window (about 54 m x 54 m) which is the minimum-sized window to guarantee a reasonable signal to noise ratio. We could not detect the glacier speed up in the narrow region near the front even with the smaller size window (Fig. 2.7). The band of ice speed near the ice front is therefore uniquely revealed in the GPRI data using the interferometric phase at the 5 m spacing.

2.3.4 CTD Analysis

We were able to complete 7 full CTD transects of 12 casts each, locations shown in Figure 2.8. The time series of data showed relatively stable measurements in the fjords over a period of several weeks, with no major daily variability in temperature, salinity, and dissolved oxygen. Figure 2.9 shows each variable average over the 7 casts. The temperature profile at the glacier front (Figure 2.9a) suggests that warm Atlantic ocean water does not reach the ice front. Our CTD measurements show that the coldest ocean water is at the bottom of the fjord, with a warmer layer above and a very thin layer of colder water near the surface. This thin cold surface layer may be the subglacial meltwater residing above the saltier and more dense ocean water. There is no evidence of Atlantic warm water in the deepest part of the fjord found from our CTD transect.

2.4 Discussion

Sub-daily acquisitions give insights into the complex temporal dynamics of the glacier. From the time series of satellite data, we detect strong inter-annual, seasonal and weekly variations but gain no insight about daily variations. Averaged over several days, the TSX and GPRI measurements agree but miss the impact of tides and calving events on glacier dynamics

(Fig. 2.3A-C).

The influence of tides on glacier velocity has been studied in Greenland and Antarctica with differing results. Rutford Ice Stream varies in-phase with the tides at fortnightly timescales with the highest speeds at spring tide and lowest at neap tide (Gudmundsson, 2006). Conversely, Helheim and Jakobshavn Glaciers in Greenland and LeConte Glacier in Alaska have out-of-phase relationships with tidal height (O'Neel et al., 2001; Davis et al., 2014; Voytenko et al., 2015; Holland et al., 2016; Podrasky et al., 2014; Cassotto et al., 2018), contrary to what we observe at Kangilernata Sermia. Non-linear responses to changes in tidal height have been noted for glaciers with floating ice shelves (Brunt et al., 2010; King et al., 2010; Makinson et al., 2012; Padman et al., 2018). A GPS survey of Helheim glacier reported a daily cycle upstream of the glacier terminus attributed to enhanced sliding caused by meltwater production (Holland et al., 2016). With only daily averaged runoff data available, we find no such relationship between 12-hour or 24-hour stacked GPRI derived ice velocity and runoff for Kangilernata Sermia. It would be of interest to future studies to compare ice velocity with higher temporal resolution runoff values.

Calving events observed on tide-water glaciers, including with GPRI, do not always affect glacier speed (Voytenko et al., 2015; Podrasky et al., 2014; Cassotto et al., 2018). Our observations reveal that only the detachment of full-thickness grounded ice blocks affect the glacier speed, which was only possible to verify because of the high quality bathymetry data at the glacier front. In addition, we find that the change in speed only affects the area near the ice front, not extending far inland, typically about one ice thickness. This finding is consistent with the glacier force balance analysis that dictates that ice blocks already afloat in the ocean have no effect on basal resistance or lateral drag, hence should not affect the glacier speed when removed, whereas grounded ice blocks will reduce basal resistance when they detach from the ice front. This effect has been observed using GPRI data at both Jakobshavn Isbrae (Cassotto et al., 2018) and Helheim Glacier (Holland et al., 2016)

without the support of high quality bathymetry. We posit that for these glaciers as well, the calving events that affected glacier speed must have involved the detachment of blocks of grounded ice.

In the ensuing hours and days following the calving event, the glacier speed in the proximity the calving event did not return to its original state. But the effect only propagated over short distances. We posit that the time it takes for the glacier to resume its original speed at the ice front is equivalent to the time it takes for new piece of grounded ice to come replace the detached piece of grounded ice, here equivalent to a period of 2 to 3 weeks at the current glacier speed, which is similar to the time scales reported in other studies (Cassotto et al., 2018). The lack of speed up upstream of the ice front indicates that the stress coupling between the ice front and the remainder of the glacier decays quickly, within one ice thickness.

The analysis of strain rates reveals the presence of a narrow band of high stresses near the ice front where calving occurs. Morlighem et al. (2016) uses a calving law based on the von Mises (VM) stress. Choi et al. (2018) compared different calving laws and concluded that the VM calving law produced the best fit with observations. In that approach, calving occurs when the tensile stress exceeds a threshold σ_{max}. Here, we use a deformation constant of 324 kPa/yr$^{1/3}$ (value for ice at -5°C, with an uncertainty of 25% (Cuffey and Paterson, 2010)) to convert the strain rates into stresses. With this selection of deformation constant, we calculate stresses ranging from 600 to 900 kPa near the calving margin. Near the largest calving event, the tensile stress was 700 kPa (Fig. 2.1E), which suggests σ_{max} values close to the breaking strength of ice at 1 MPa. In contrast, near the ice front, satellite measurements indicate stress values that remain below 500 kPa, i.e. which largely underestimate the peak stresses. A low value of 500 kPa for σ_{max} would overestimate calving rates if employed in a numerical model. We recommend that other glaciers be examined in a similar fashion to evaluate σ_{max}. Caution should be exercised when interpreting strain rate records based

on coarse resolution velocity measurements from speckle tracking or optical tracking that average data over many hundreds of meters.

The application of optical and radar satellites has been transformative for mapping ice velocity in Greenland and Antarctica. GPRI studies reveal important information missing from these measurements. In particular, glacier speed up after a calving event is no longer detectable if data averaging exceeds 3 hours (Fig. 2.7) and spatial details of the stress field at the ice margins are missing from speckle tracking using satellite data with a long repeat cycle. These findings reinforce the need to track ice motion using the interferometric phase at the pixel level instead of speckle tracking. In order to do so, satellite data must be acquired at much shorter time scale, and typically sub-daily. While GPRI is useful to examine processes taking place at that temporal scale, it can only be deployed on a few glaciers over limited periods of time without protection from wind and weathering and without securing of long-term energy supply.

2.5 Conclusions

We present the first sub-hourly observations of speed and elevation of Kangilernata Sermia in western Greenland using GPRI to investigate its calving dynamics. We find that the glacier experiences strong diurnal velocity fluctuations of 20% that are positively correlated with tidal pressure and that affect the entire glacier far inland. In contrast, the only calving events that affect glacier speed are those that remove full-thickness grounded ice blocks. While the change in speed consecutive to a large calving event persists for days, consistent with other studies, and extends to a large region around the zone of detachment, the effect does not propagate far inland, hence does not have a major impact on glacier dynamics. In terms of deformation rates, we detect strain rates and stresses 2 to 3 times larger than reported previously along calving fronts using satellite measurements, which has implications

for understanding and modeling the break up of ice into icebergs.

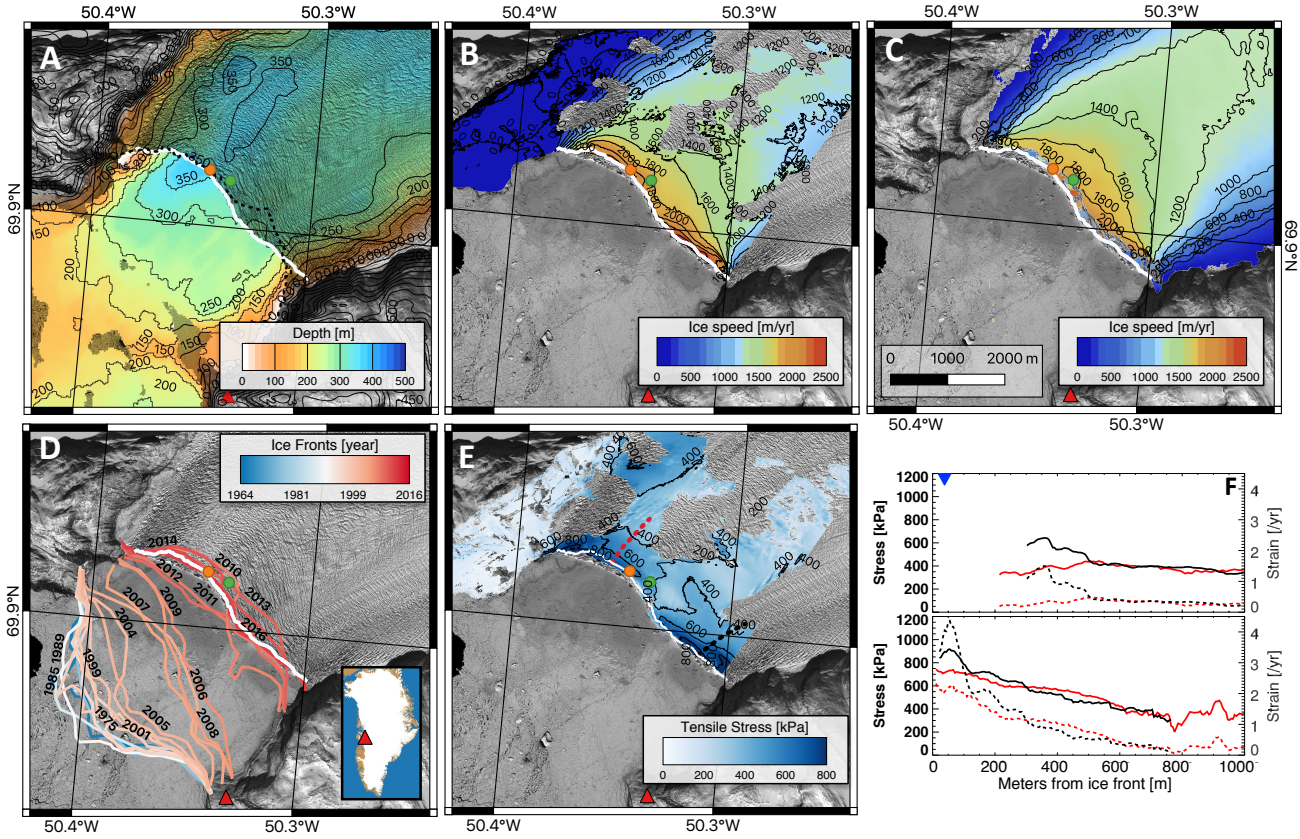

Figure 2.1: Kangilernata Sermia, Greenland with A) OMG bathymetry and BMv3 bed elevation, black-dashed line marking the limit of the 2012 MBES coverage beneath the glacier in 2016. B) GPRI-derived ice speed with contours every 200 m/yr, C) TerraSAR-X-derived ice speed with contours every 200 m/yr, D) historical ice front positions from 1964-2016, E) tensile strain rate calculated from GPRI with contours every 200 kPa, and F) tensile stress (solid line) and strain rate (dashed line) along red dashed profile (Fig. 2.1E) from GPRI (black) versus TerraSAR-X (red), with ice front after the large calving event (Fig. 2.5A) denoted as blue inverted triangle. Ice front location on 05 July 2016 is white. Green dot is the location for the time series in Figure 2.3. GPRI is located at red triangle.

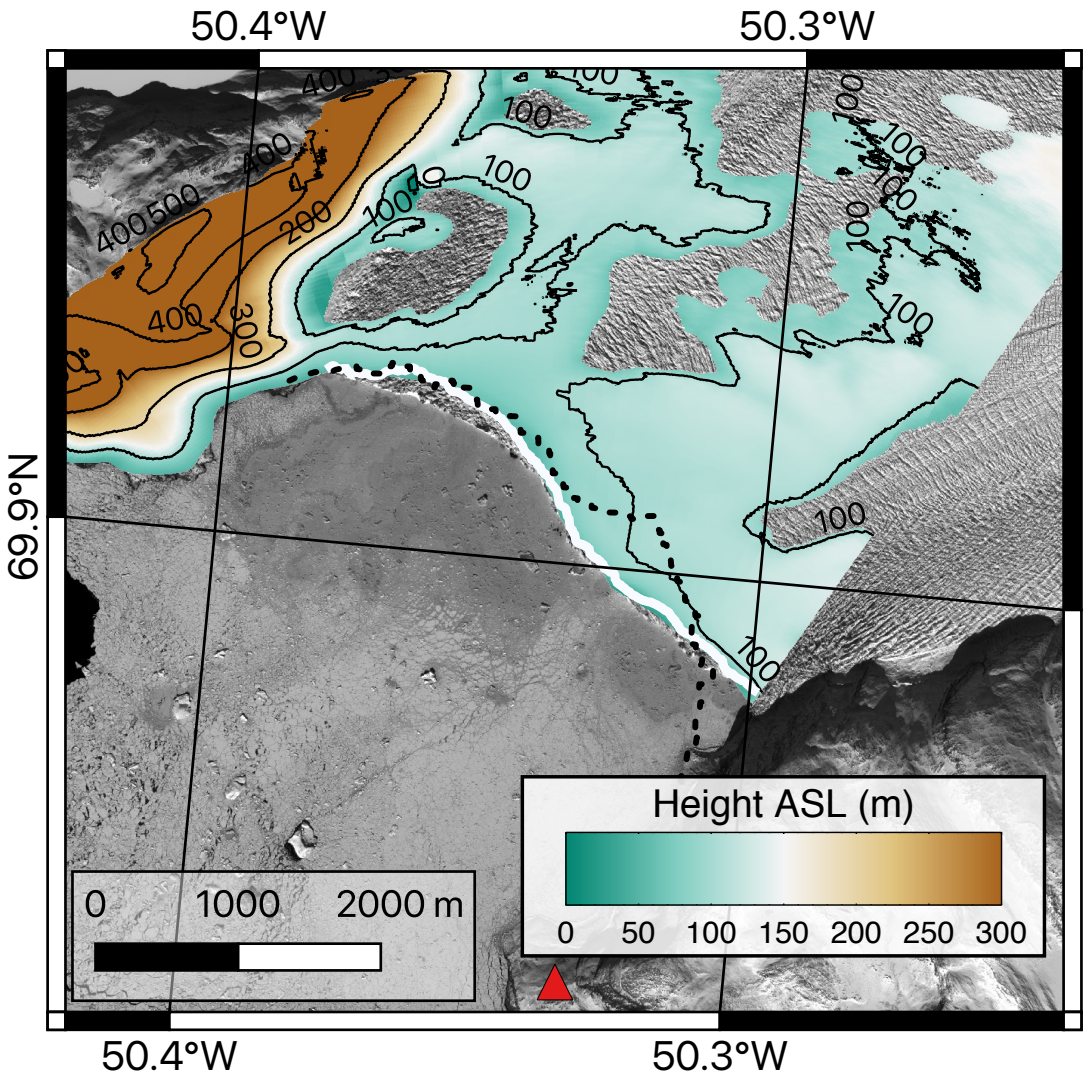

Figure 2.2: GPRI-derived DEM in meters above sea level. Black dashed lines outline the inner limit of where MBES data exists beneath the glacier. Ice front location on 05 July 2016 is white. GPRI is located at red triangle.

Figure 2.3: HOBO U20 Water Level Logger used to measure water pressure in both 2016 and 2018 field campaigns. Photo courtesy of OnSet (https://www.onsetcomp.com/).

Figure 2.4: Photos of CTD deployment via inflatable zodiac boats. Photos taken by Jeremie Mouginot.

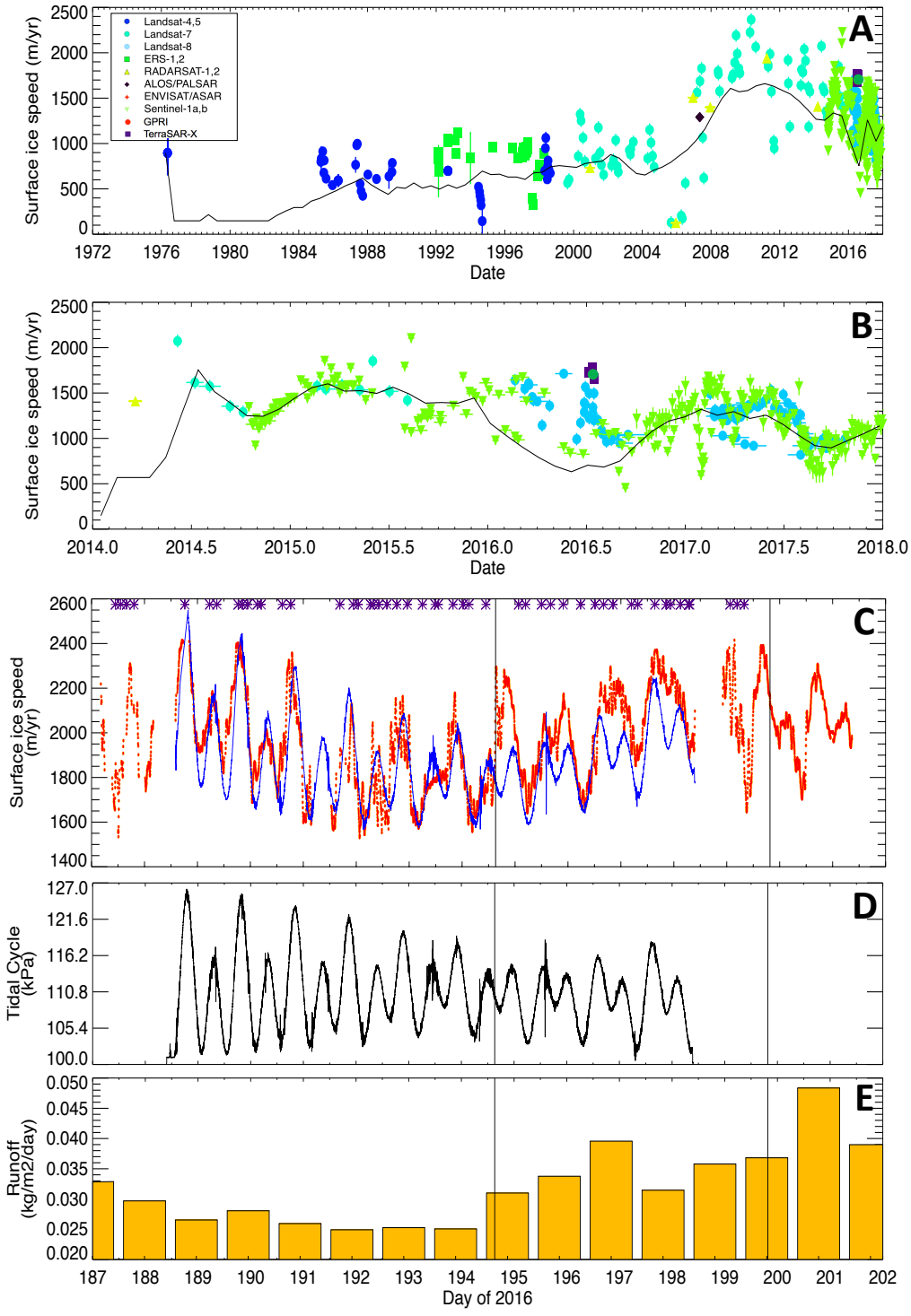

Figure 2.5: Time series of ice velocity for Kangilernata Sermia, Greenland derived from A) satellite data for 1976-2018 and B) for 2014-2108, with GPRI in red. C) GPRI-derived velocity for 5 July 2016 - 19 July 2016 in red versus tidal forcing from a model in blue. Purple stars denote timing of small shedding events. D) Tidal amplitude in kilo Pascal (kPa) E) daily average runoff from the RACMO2.3 surface mass balance model. Black vertical lines indicate two large calving events examined in Fig. 2.5.

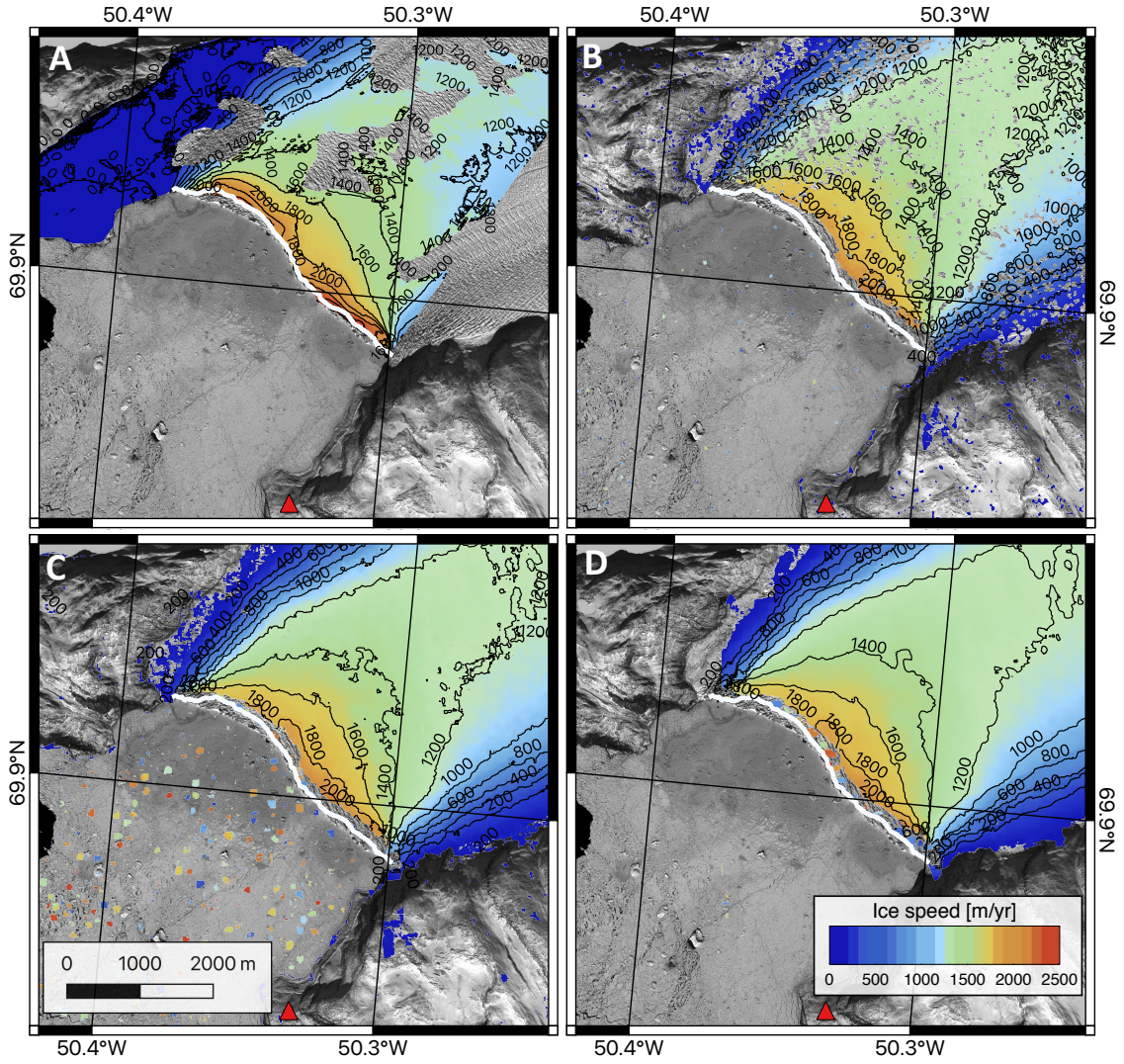

Figure 2.6: Ice speed of Kangilerngata Sermia, Greenland, with A) GPRI, B) TerraSAR-X derived ice speeds from acquisitions 02 July 2016 and 13 July 2016 processed with a window of 32x24 pixels, C) 64x48 pixels, and D) 128x96 pixels. Ice front on 05 July 2016 is white. GPRI is located at red triangle.

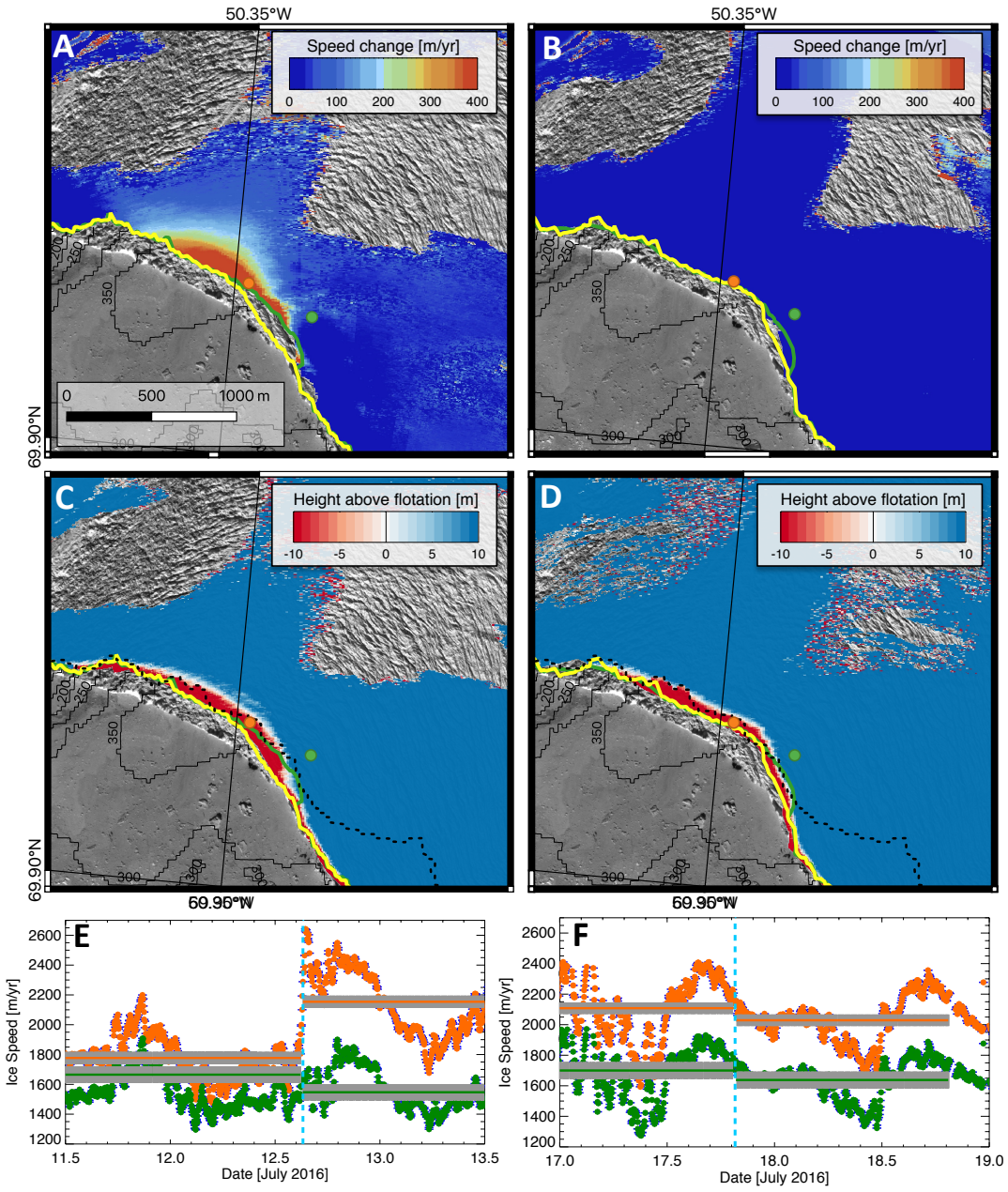

Figure 2.7: Change in velocity of Kangilernata Sermia for A) calving event on 12 July 2016 and B) 17 July 2016, with the height above floatation before the calving event in C) and D), respectively. E-F) Change in speed plotted as the difference in average speed 1 hours before and1 hour after calving. Bathymetry shown with black solid contours. Ice front positions before and after the calving events are colored yellow and green, respectively. Black-dashed line outlines where MBES data exists under the glacier. E) and F are 30-minute-averaged GPRI-derived ice speed at the yellow dot in A-D around each calving event (cyan dashed line). Black line showing 24 hour average ice speed before and after calving events with grey bar outlining error. Note that the yellow dot in this figure is located closer to the calving front than the green dot in Figure 2.1.

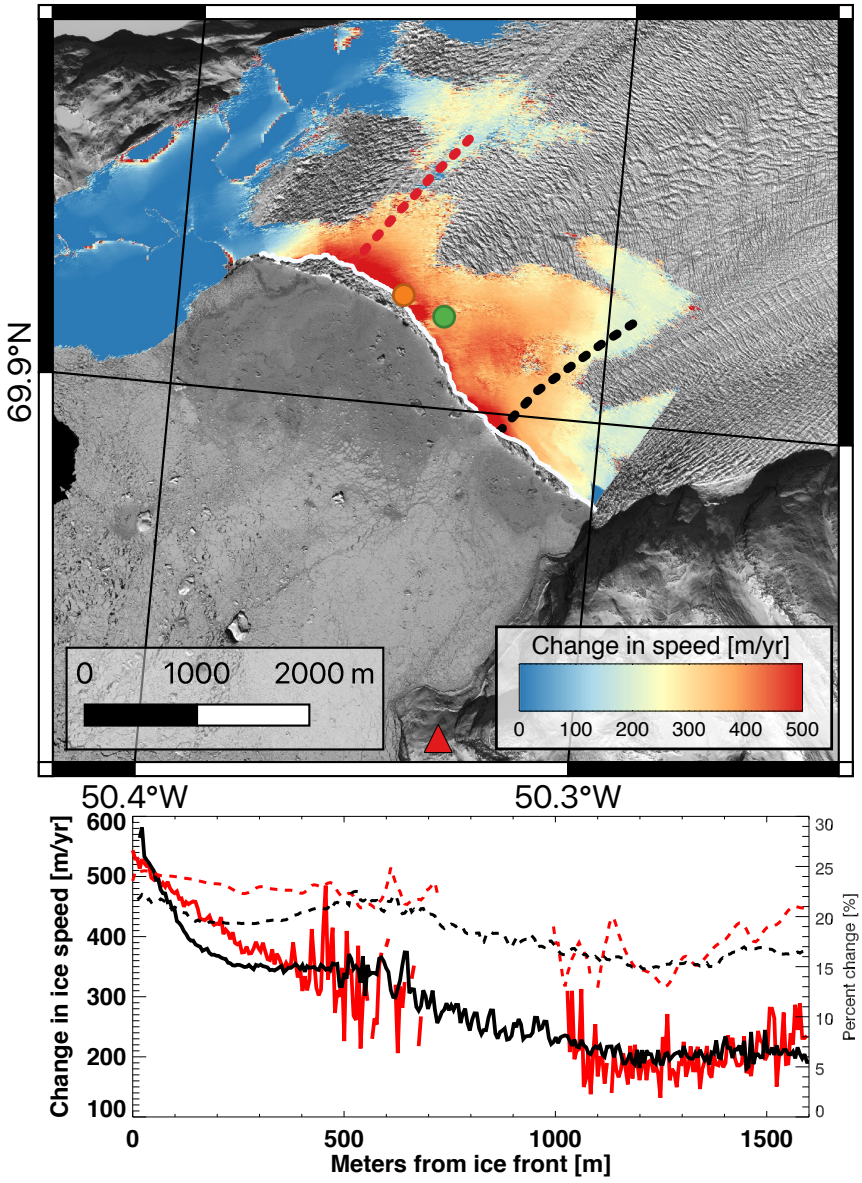

Figure 2.8: Top panel shows change in ice speed from low tide to high tide on 14 July 2018 (DOY 195). Red and black profile lines are plotted on bottom graph in red and black, respectively. Solid lines show change in ice speed in m/yr, dashed lines show percent change.

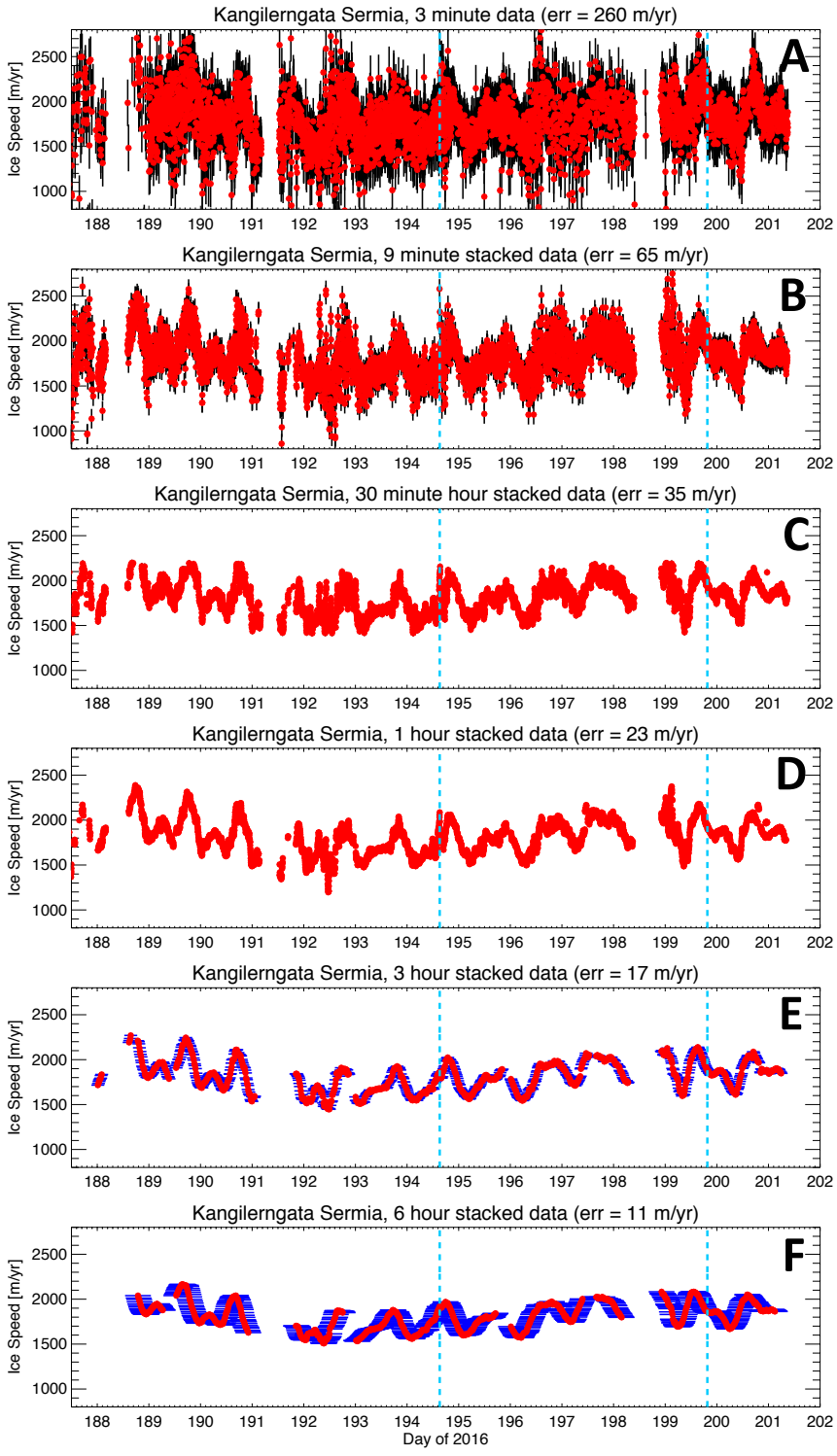

Figure 2.9: Time series of GPRI-derived ice speed with A-F as showing 3, 9, 30, 60-minute, 3 hour, and 6 hour stacked data, respectively, plotted in red with vertical error bars in black and horizontal errors in blue. Cyan dashed lines indicate timing of major calving events discussed in Figure 2.5.

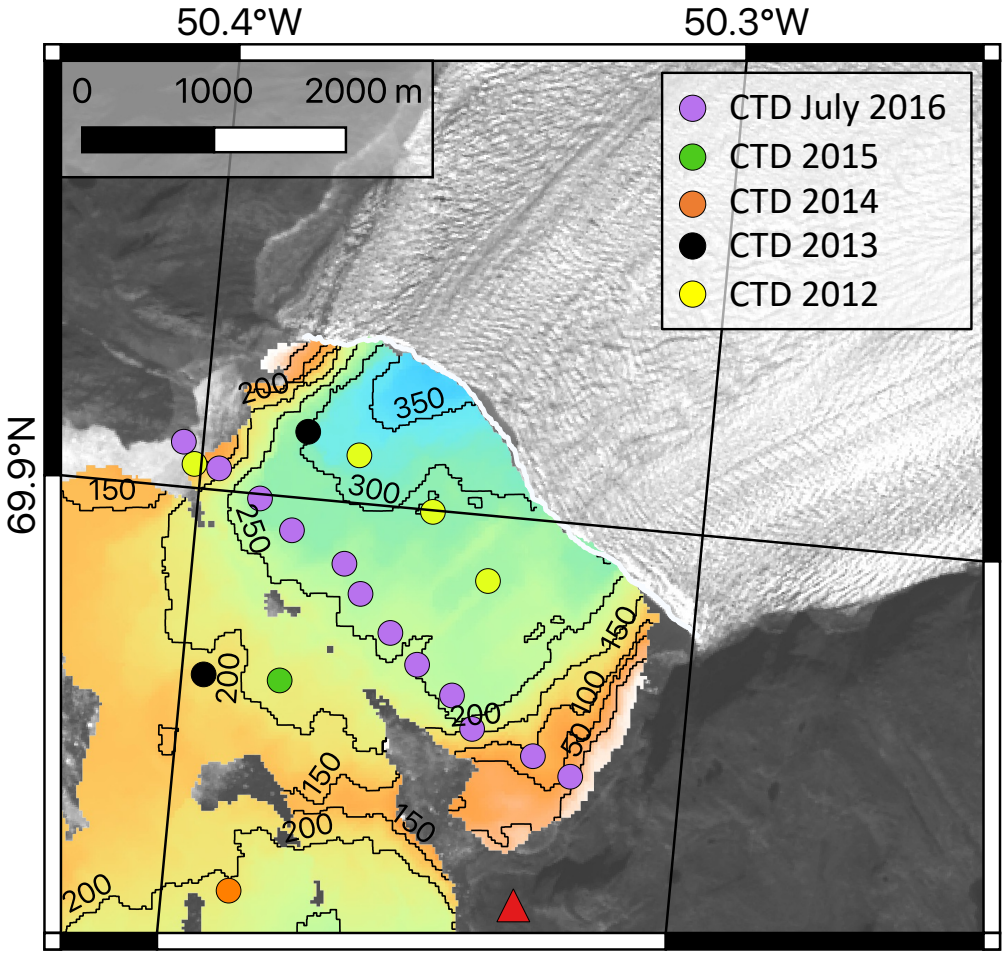

Figure 2.10: Locations of 12 CTD casts taken during the July 2016 field campaign at Kangilernata in purple. Other CTDs taken in various years as part of NASA's OMG campaign plotted according to color.

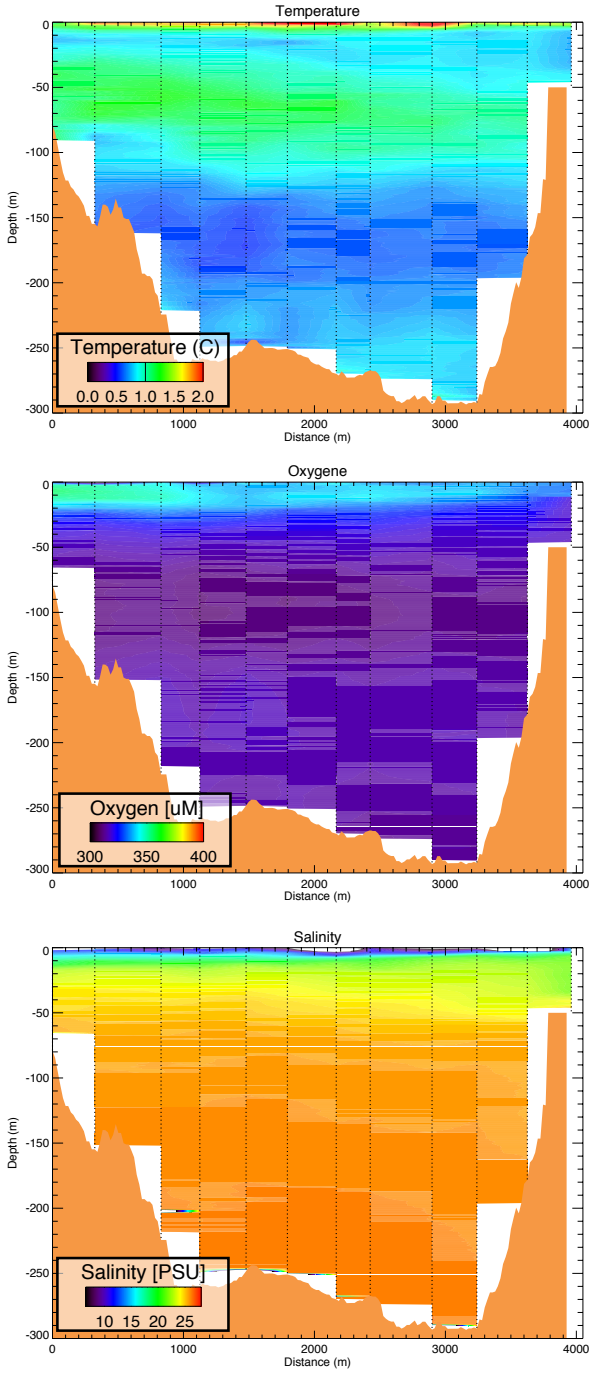

Figure 2.11: Averaged results of CTD surverys showing temperature, dissolved oxygen, and salinity in the fjord. Casts taken 1.5 km from the ice front of Kangilernata, shown in figure 2.8

Chapter 3

Calving dynamics in Torsukataq Fjord, Greenland

3.1 Introduction

Sermeq Avanarleq (AVA) and Sermeq Kujalleq (KUJ) are two calving-dominated (Wood et al., 2018) marine-terminating glaciers that drain into Torssukatak Fjord in central western Greenland. AVA, located at 70°3′N, 50°19′W, drains an area of 7,958 km^2 with a center speed of 1.5 km/yr at the ice front. KUJ, located at 69°59′N, 50°10′W, drains an area of 18,263 km^2 with a center speed of 3.0 km/yr (Rignot and Mouginot, 2012). Based on BedMachine Version 3 (BM3), these glaciers have a sea level rise equivalent of 4.4 cm and 10.9 cm, respectively. Seasonal variations in ice speed have been observed at both glaciers in recent years (An et al., 2018).

AVA has been a stable glacier since 1903, with ice front position changes of less than 100m since (Wood et al., 2018). Avannarleq is grounded at a shallow area with more than half of the ice front at a depth of less than 200 m (Fig. 3.1A). The front is grounded at 300 m

below sea level at the deepest. The bed increases with depth up to 500 m below sea level just 800 m upstream of the current ice front position.

KUJ has been much more active than AVA with retreat of more than 2 km from 1851-1949, followed by stable conditions until 1961 when the glacier retreated another 700m in 4 years (Anker Weidick, 1968), with a second period of retreat covering 1.5 km from 1997-2001 (An et al., 2018). A sill up to 300 m below sea level exists about 1500 m from and almost parallel to the current ice front position (Fig 3.1A). The glacier is grounded at its current location at a depth of up to 400 m below sea level with the deepest part of the bed at the center of the glacier front. The bedrock beneath the center of the glacier continues to increase in depth upstream up to 500 m below sea level 2500 m inland.

Here we present the first sub-hourly study of the calving fronts in Torssukatak Fjord using GPRI data collected in July 2018. We relate changes in ice speed to changes in the ice front position, calving events, and the tidal cycle. We conclude on the importance of high temporal resolution data collection for understanding marine-terminating glacier dynamics and the future of ice sheet modeling.

3.2 Materials and Methods

3.2.1 Satellite data and bathymetry

We assemble satellite-derived velocity measurements of Avannarleq and Kujalleq from 1984 to present using Landsat-4,5,7,8, ERS-1,2, RADARSAT-1,2, ALOS/PALSAR, ENVISAT/ASAR, Sentinel-1a,b, and TerraSAR-X (Mouginot et al., 2017). The temporal resolution of the data depends on the native repeat cycles of these satellites, which ranges from 6 for Sentinel-1a/b to 44 days for ALOS PALSAR. We extract velocity values at various points along the 2018

front of Kujalleq and Avannarleq glaciers and upstream. We compare GPRI derived velocity with the existing satellite data set using a point 1 km from the ice front (Fig. 3.1). Historical ice front positions at both glaciers (Wood et al., 2018) show the ice front locations back to the 1980s (Fig 3.1D).

Fjord bathymetry was mapped with multibeam echo sounding (MBES) in September 2016 to constrain bed elevation to within 1 m up to the ice front at Avannarleq and up to about 1200 m from the ice front of Kujalleq. This MBES data combined with bathymetry calculated from gravity anomalies (An et al., 2018) allow for a full picture of the bathymetry in the fjord in front of these two glaciers (Fig. 3.1A).

3.2.2 GPRI

We deployed a GPRI at Torsukatak Fjord between 3 July - 14 July 2018 with few multi-hour breaks due to high wind and/or heavy rainfall (Figure 1.1). The GPRI was situated at 113 m above sea level for the entire field campaign, 3,400 m from the center of Kujalleq's ice front and 7,700 m from the ice front of Avannarleq (Fig 3.1 and 3.2). Data was acquired every 3 minutes with few multi-hour breaks due to high wind and/or heavy rain.

Due to lack of flat, high ground for GPRI placement, the instrument was deployed at an elevation causing a low grazing illumination angle. This low grazing illumination angle placed some sections of the ice surface upstream of the ice front in the shadow of the radar illumination, yielding no signal in these areas.

GPRI data is stacked to reduce noise without unnecessary temporal averaging. Noise values of GPRI-derived ice speed ranges from 250 m/yr for 3 minute data to 6 m/yr for 12 hour data (Fig. 1.2, 3.3). We use 30 minute stacked data, with a error of 37 m/yr, for the analysis of both glaciers.

3.2.3 Tracking Calving Events

Geolocated ice front positions are created from the multi-looked radar backscatter intensity (MLI) at each acquisition (Fig. 3.4). This MLI imagery is also used to view the motion of icebergs and melange in the fjord with time. Calving events and shedding events are tracked and classified in the same manner as in Chapter 2.2.3 with calving events defined as causing a change in ice front position while shedding events cause no change in position.

3.2.4 Tidal Measurements

We installed a HOBO U20 Water Level Logger for 9 days to collect water pressure measurements and allow for tidal height calculations. The tide gauge measured pressure below the water line at a site about 10 km away from the ice front.

3.3 Results

3.3.1 Velocity analysis

The time series of satellite derived ice speeds begins in 1984 for both Kujalleq and Avannarleq glaciers. Avannarleq has remained stable, flowing between 1,500 and 2,000 m/yr at a point 1 km from the ice front (Fig. 3.5A). Kujalleq has remained stable at a higher speed of between 4,000 and 5,500 m/yr (Fig. 3.5E). Zooming in on these time series displays the seasonal variability in ice speed at each glacier (Fig. 3.5B and 3.5F). Avannarleq's seasonal ice peak occurs in summer with ice speeds up to 2,000 m/yr, followed by minimum ice speeds between 500-1,000 m/yr in fall/winter (Fig. 3.5B). Kujalleq's seasonal cycle peaks close to 5,000 m/yr in late summer/fall with minimums near 3,000 m/yr in late winter (Fig. 3.5F).

The average of the GPRI-derived ice speeds match well with the available satellite data (Mouginot et al., 2019) (Fig 3.5, 3.6). Ice speeds at Avannarleq glacier remained steady throughout the 11 day July field campaign, flowing at 2,050 m/yr on average. Over the time period of observation, Kujalleq glacier responded to tides, calving events, and subglacial runoff. Over the first 4 days of data collection the glacier averaged 7,400 m/yr at the ice front, with an increase over 08-10 July and re-stabilizing at an average of 8,100 m/yr for the last 3 days of observations (Fig 3.5G).

Throughout the field campaign, Kujalleq was modulated by the tidal cycle, with diurnal velocity changes of up to 8% and an overall correlation of 0.34 at the 95% significance level. No correlation was found between the ice front speed at Avannarleq and tidal cycle.

3.3.2 Calving event analysis

During our period of observation, we determined from the MLI imagery that 19 events fit our definition of calving, with 8 from the front of Avannarleq and 11 from the front of Kujalleq (Fig. 3.5C and 3.5G). Many smaller events determined to be shedding events occurred at both glaciers throughout the study period. Of the 8 calving events at Avannarleq, none of them caused any change in glacier speed.

Two of the 11 events at Kujalleq were determined to be one event that occurred in two parts, referred to part 1 and part 2 throughout the rest of this study. This 2 part calving event was the only event to cause a localized change in ice speed of about 16%. Part one occurred on 09 July 2018 (DOY 190). The ice block began to detach at 22:14 UTC and took 9 minutes to break off completely. The block was 700 m wide and 200 m long at its largest and broke into two pieces as it calved and was pushed away from the ice front (Fig. 3.7). The peak ice speed increased from 8,050 to 9,100 (13%) after part one of this event (Fig. 3.7D). The speed up is localized and does not propagate far upstream. An increase of at least 10% extended

1200 m along the ice front and 500 m upstream.

Part 2 occurred about 7 hours later at 05:02 UTC on 12 July 2018 (DOY 191). Ice speed further increased to a peak of 9,300 m/yr (16%) after part 2 of this event (Fig. 3.7). Part two removed a block of ice 1200 m wide and 300 m long. The speed increase spread farther in all directions, with an increase of at least 10% extending 1400 m along the front and 700 m upstream (Fig 3.7E). The full calving event, parts one and two combined, removed an area of 1800 m along the ice front and 300 m upstream.

The interferometric fringes allow for the linking of these two events as one calving event, despite the 7 hour time difference. Decorrelation of the entire calved area is visible 1.5 days before event part 1 (Fig. 3.8).

3.4 Discussion

GPRI studies with a temporal resolution of less than one hour reveal important information about the dynamics of marine-terminating glaciers that is not observable with traditional satellite data and processing. Current satellite data processing utilizes speckle-tracking methods rather than interferometric phase used to process GPRI data. Figure 3.6 shows the comparison on data coverage of TerraSAR-X, GPRI, and the satellite data composite map from (Mouginot et al., 2017, 2019). While limited in spatial coverage, GPRI has the unique ability to image the entire glacier front using interferomteric phase, allowing for unwrapping and LOS to velocity conversion of the glacier up to the ice front. Satellite data with repeat pass times of a week or more cannot recover information at the ice front, as a portion of the ice front is lost between acquisitions due to shedding, calving, and/or melt. It is impossible to map the glacier speed right up to the ice front using measurements with repeat pass times of more than a few days. The tracking algorithms used to process satellite data use image

chips of large areas (several tens of pixels) for correlation. The size of these image chips limits the ability to map sharp gradients in speed at an ice front or shear margin.

The spatial coverage of the GPRI also allows for calculation of strain rate and stresses up to the ice front in the same manner as described in Chapter 2.4. This cannot be done with currently available satellite data. We detect higher than expected strain rates at the ice front, with values over 4.5 yr^{-1} (Fig. 3.1). These high strain rates at the ice front change our understanding of the σ_{max} value to be used in calving models. A value lower than observed here would overestimate calving rates in a numerical model.

The influence of tides on glacier velocity has been shown to have differing results from glacier to glacier. Glaciers such as Helheim and Jakobshavn Glaciers in Greenland and LeConte Glacier in Alaska have out-of-phase relationships with the tidal cycle (O'Neel et al., 2001; Davis et al., 2014; Voytenko et al., 2015; Holland et al., 2016; Podrasky et al., 2014; Cassotto et al., 2018), with high ice speeds at low tide. These studies support the out-of-phase relationship found with Kujalleq ice speed and tidal height.

The relationship between calving and glacier speed has been studied at multiple marine-terminating glaciers in Greenland (Voytenko et al., 2015; Podrasky et al., 2014; Cassotto et al., 2018), (Kane et al., 2020). Our findings here are consistent with those of other marine-terminating glaciers that state not all calving events cause a change in glacier speed (Voytenko et al., 2015; Podrasky et al., 2014; Cassotto et al., 2018) (Kane et al., 2020). One two-part calving event out of a total of 10 observed calving events at Kujalleq caused a speed increase of 16%. The pattern of speed increase was localized, centered around the calved area and extending only 1800 m along the ice front and 700m upstream. This differs drastically from the pattern of ice speed change caused by changes in tidal height which are less extreme and extend over a much large area of the glacier. This finding is consistent with the idea that ice blocks already afloat in the ocean have no effect on basal resistance or lateral drag, which comes directly from the glacier force balance analysis. Removal of

floating ice causes no change in force balance, and does not effect the glacier speed. Removal of grounded blocks of ice lower basal resistance, therefore causing the glacier to increase in ice speed. This effect is clearly seen on Kangilernata Sermia and described in Chapter 2 and (Kane et al. 2020, submitted).

The two part calving event at Kujalleq must have removed a significant portion of grounded ice to cause the observed localized ice speed increase. This effect has been measured (Kane et al. 2020) and presumed (Cassotto et al., 2018; Voytenko et al., 2015; Podrasky et al., 2014) at other marine-terminating glaciers in Greenland. Without available high-resolution bathymetry data, determining where along the ice front is grounded vs. floating is not possible. These calculations require high-resolution ice thickness data, which is dependent on the time series of GPRI-derived DEMs and high-resolution bathymetry measurements. At Kujalleq, MBES data stops about 1,400 m from the ice front due to a high concentration of thick melange during the time of data collection. This effect has been observed using GPRI data at both Jakobshavn Isbrae (Cassotto et al., 2018) and Helheim Glacier (Holland et al., 2016) without the support of high quality bathymetry.

Parts 1 and 2 of this calving event occurred after a 1.5 day gradual increase in ice speed (Fig 3.4H). This speed up is likely linked to precipitation in the region and/or runoff.

3.5 Conclusions

Presented here are the first sub-daily observations of Torsukataq Fjord including both Kujalleq and Avannarleq Glaciers using GPRI. Data was collected every 3 minutes over 12 days to investigate the dynamics of the glacier fronts in the fjord. We are able to unwrap velocity and elevation data up to the ice front, increasing spatial coverage in this region drastically from what was available from satellite data. We find that the speed at the ice

front of Kujalleq fluctuates daily up to 8% in response to the tidal cycle. Out of 19 studies calving events, one two-part event at Kujalleq caused a speed increase of up to 16% at the glacier front. We find that the change in speed is highly localized, effecting only the area near the ice front where the iceberg detached. This event is two calving event linked into one by interferometric fringes. We find that the ice block began rotating away from the ice front 1.5 days before part one of the event. Part 2 removes the remainder of the rotating ice block. We infer that both parts of this event must have removed grounded ice, as both parts caused an immediate and localized speed increase.

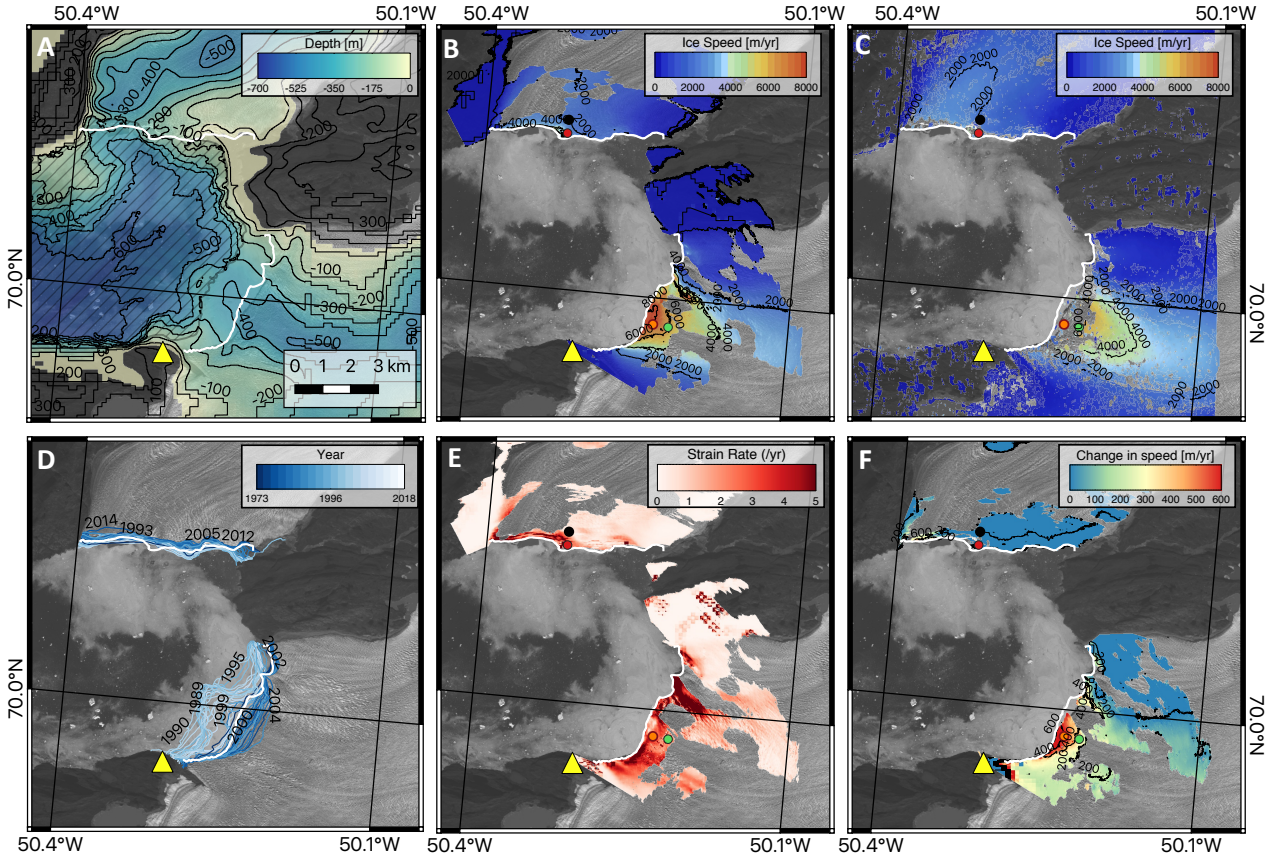

Figure 3.1: Panel A shows bathymetry and elevation. Black hashed region shows where Multibeam data from NASA's OMG Mission exists. Panel B and C show ice speed derived from GPRI and TerraSAR-X, respectively. Panel D shows historical ice fronts for both glaciers (Wood et al., 2018). Panel E and F show tensile stress and strain rate, respectively. White line denotes ice front position at the start of this field campaign. GPRI located at yellow triangle.

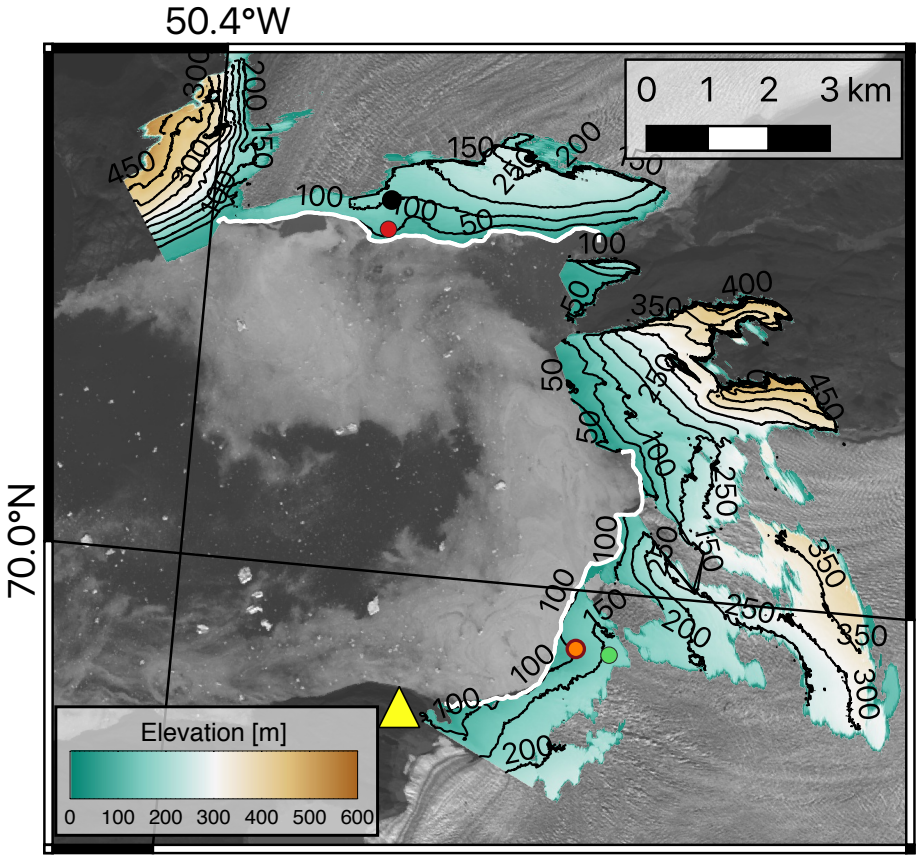

Figure 3.2: DEM derived from 30 min stacked GPRI data. GPRI located at yellow triangle. Red, black, orange, and green dots coorespond with locations used for timeseries analysis in figure 3.5.

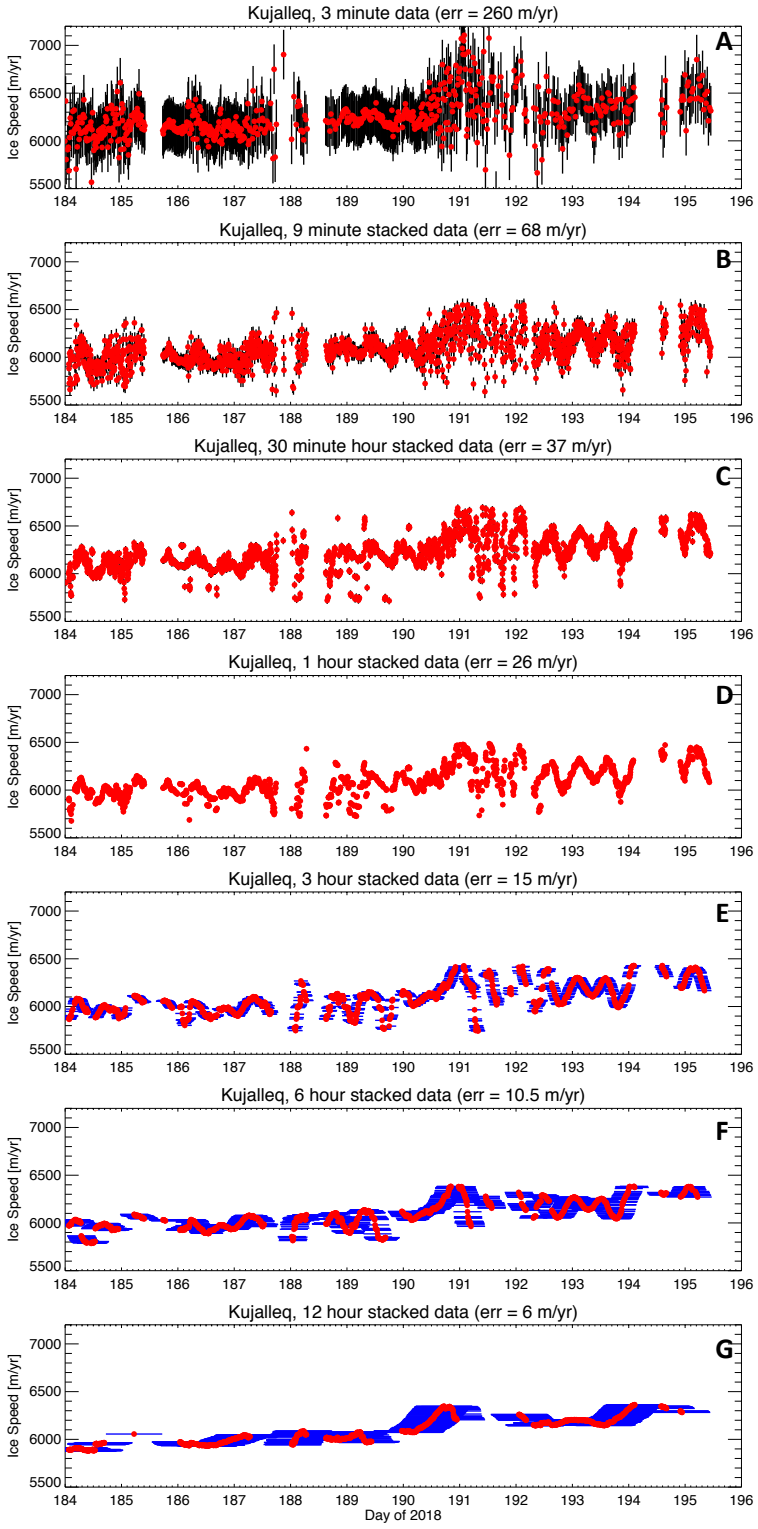

Figure 3.3: Time series of GPRI-derived ice speed with A-F as showing 3, 9, 30, 60-minute, 3 hour, and 6 hour stacked data, respectively, plotted in red with vertical error bars in black and time interval outlined in blue.

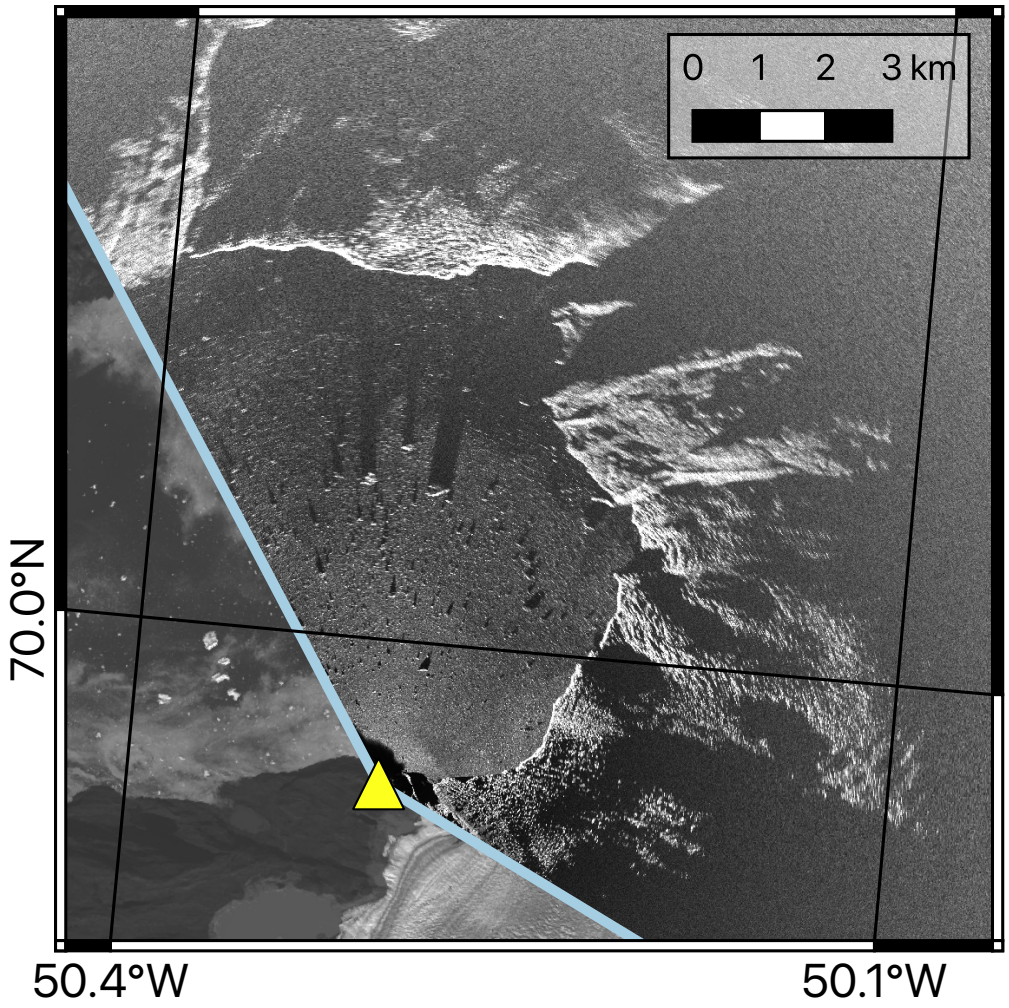

Figure 3.4: Multi-looked backscatter imagery (MLI) from 23:02 on 14 July 2018. GPRI coverage outlined in light blue with the GPRI location shown as a yellow triangle.

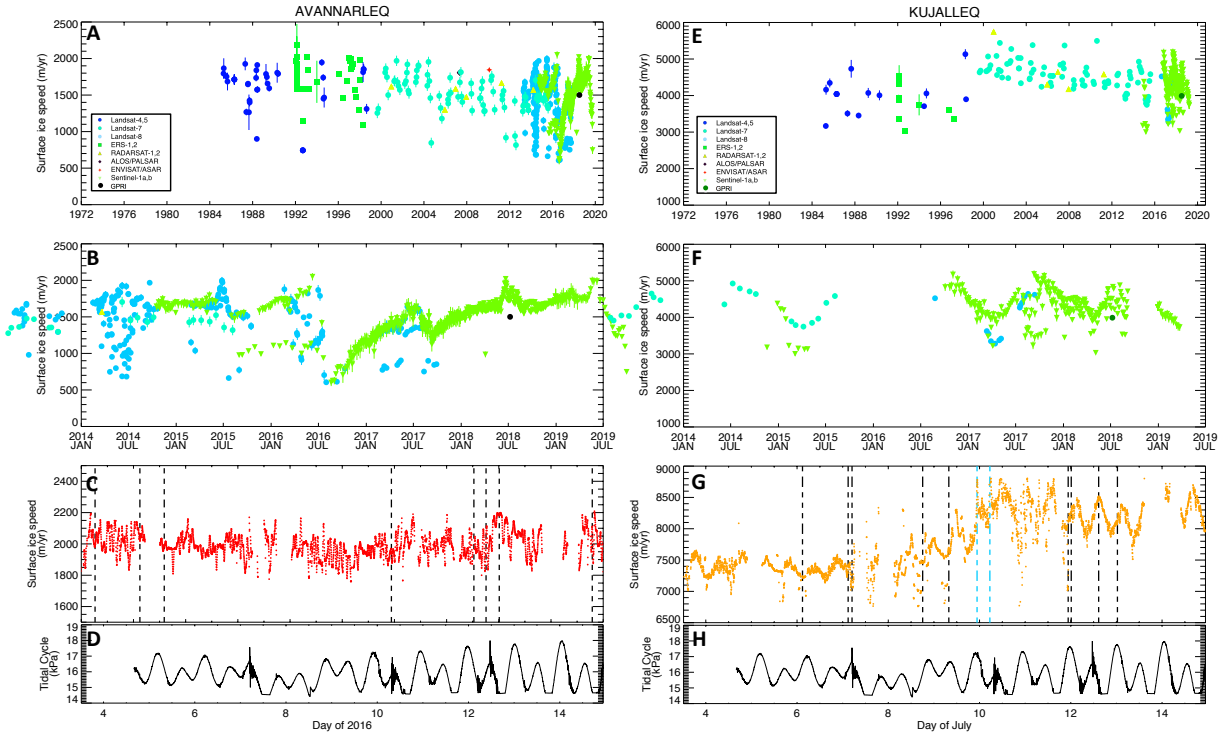

Figure 3.5: Panels A and E show time series of ice speed since 1974 for Avannarleq and Kujalleq respectively. Panels B and F shows zoomed in time series since 2014. GPRI data point is the average ice speed measured by the GPRI at the black and green points shown in Figure 1. Panels C and G show GPRI derived time series of ice speed taken at the red and orange points shown in Figure 1.

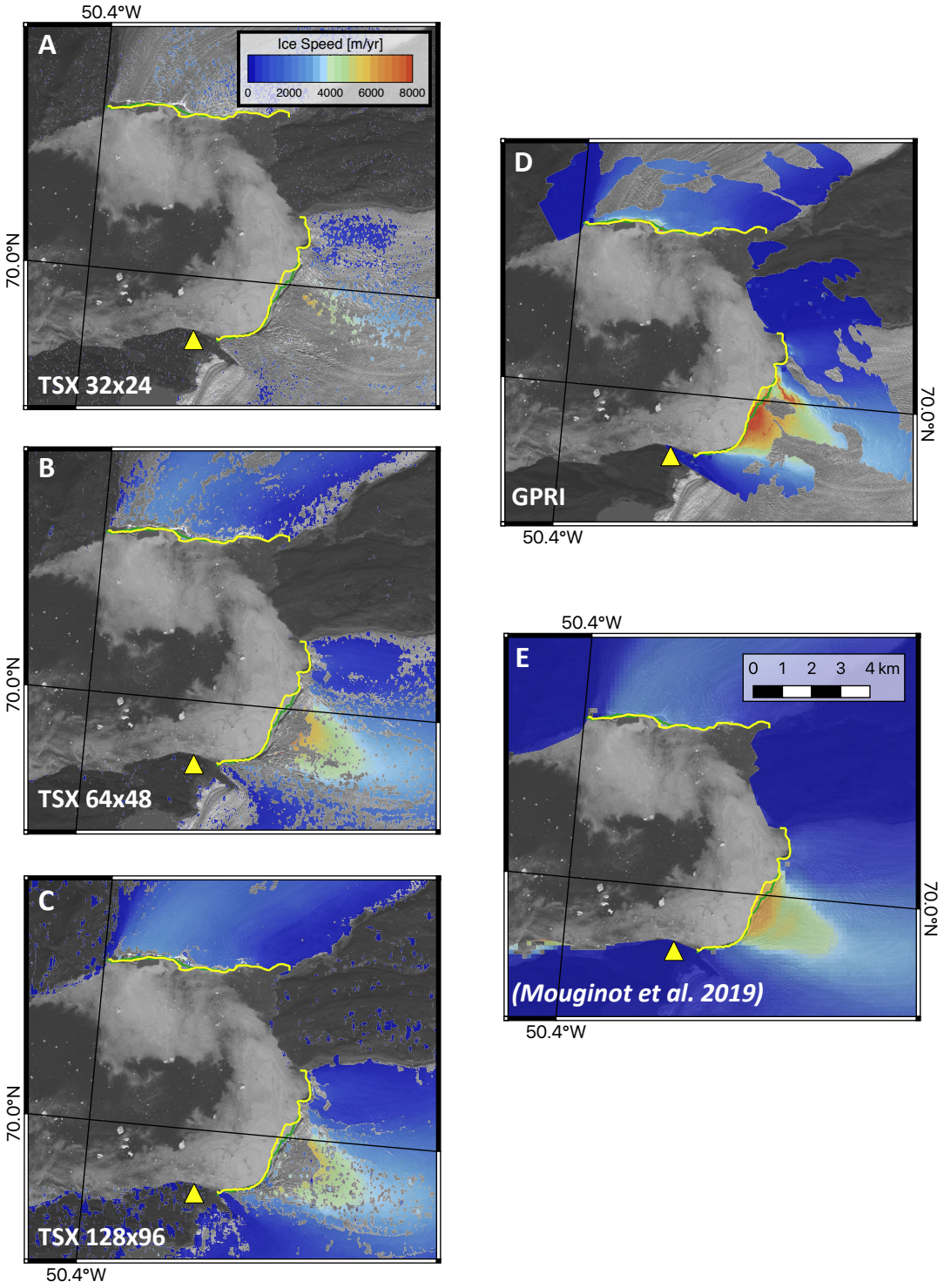

Figure 3.6: Velocity maps derived from TerraSAR-X data using a window of 32x24 pixels (A), 48x36 pixels (B), and 128x96 pixels (C). Panel D shows the GPRI derived velocity map. Panel E shows satellite derived composite map courtesy of (Mouginot et al., 2019). Yellow and green lines show the ice front positions at the start and end of this field campaign, respectively.

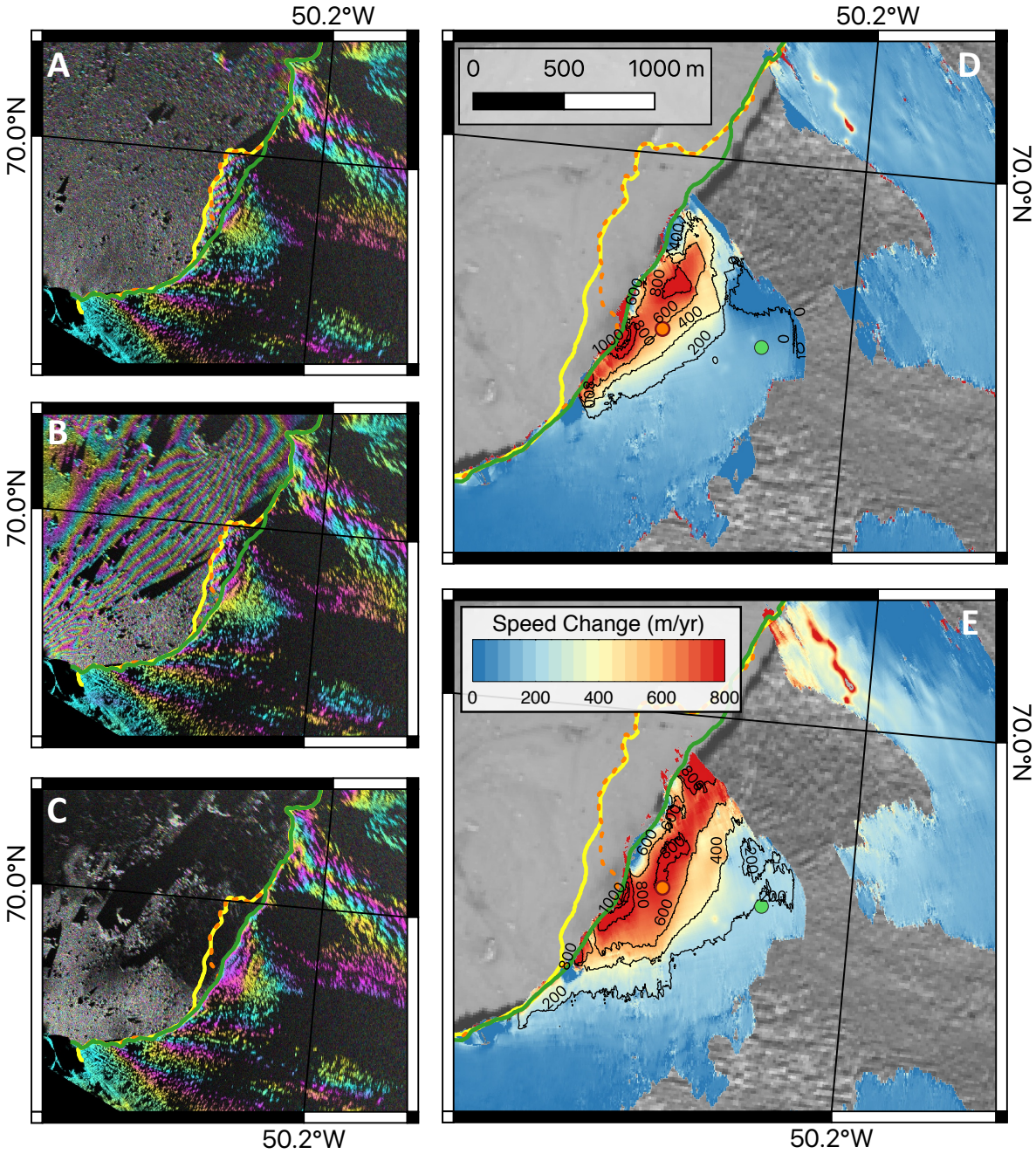

Figure 3.7: Panels A-C show interferograms before part 1 (A), after part 1 (B), and after part 2 (C) of the calving event on 09-10 July 2018. Panels D and E show ice speed change after part 1 (D) and after part 2 (E) of this calving event. Ice front position before calving denoted by yellow line, position after part 1 of the event denoted by dashed green line, and position after conclusion of the event denoted by solid green line.

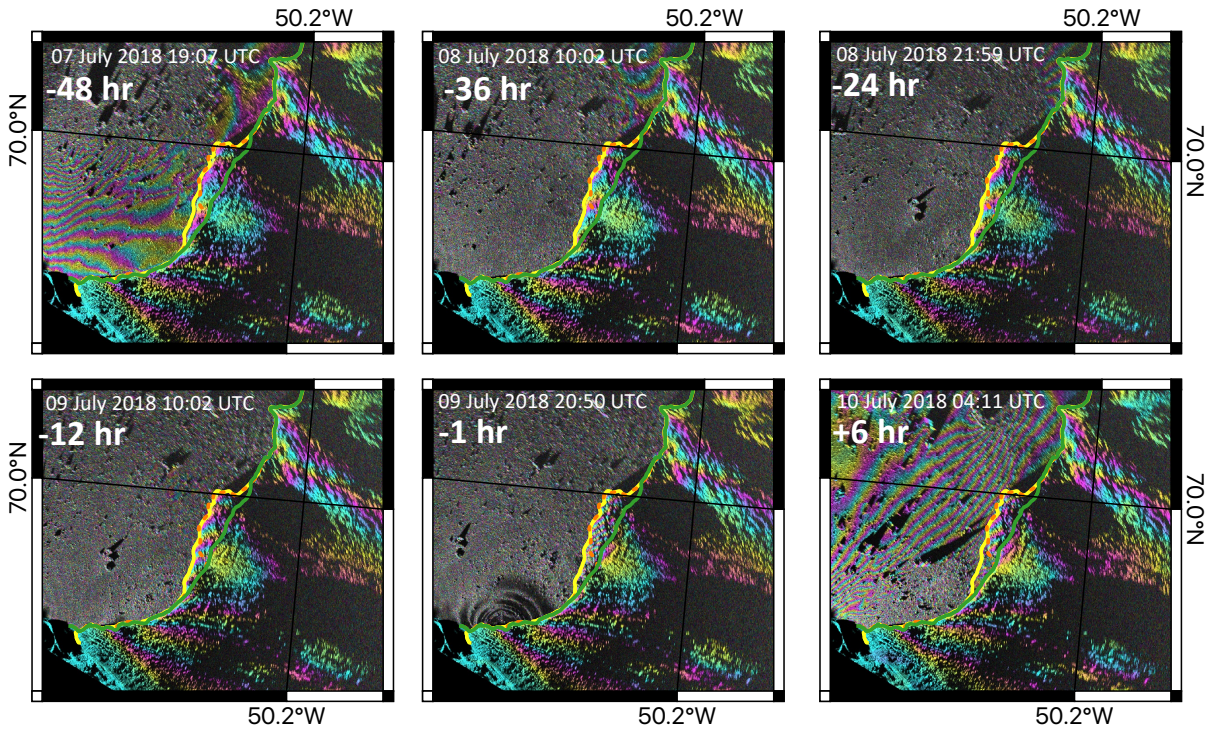

Figure 3.8: Interferograms leading up to part one of the calving event shown in Fig 3.6. Time 0 considered to be the timing of part 1 of the event. Ice front position before calving denoted by yellow line, position after part 1 of the event denoted by dashed orange line, and position after conclusion of the event denoted by solid green line.

Chapter 4

Discussion and Conclusions

4.1 Discussion

Marine-terminating glaciers in Greenland drain 88% of the ice sheet area which is comprised of enough ice to raise sea levels by 7 meters (Rignot and Mouginot, 2012). However, the full effect of climate warming on small-scale processes at marine-terminating glaciers is not well known. It is essential to understand the physical processes occurring at marine-terminating glaciers to better quantify Greenland's contribution to sea level rise. For that, it is critical to incorporate observations of short time scales with current and future satellite data sets.

Sub-daily acquisitions give insights into the complex temporal dynamics of marine-terminating glaciers. Inter-annual, seasonal and weekly variations are detected from time series of satellite data, but with this time series we gain no insight about variations on the daily (or shorter) timescale. Averaged over several days, GPRI measurements agree with available satellite measurements but miss the impact of tides and calving events on glacier dynamics. Calving dynamics are vital to accurately simulate ice sheet behavior (DeConto and Pollard, 2016), and increase accuracy of future sea level rise projections. In order to improve ice sheet

models, observations of ice front dynamics must be made on the sub-daily timescale.

The goals of this project revolved around improving our understanding of trends and variability in glacier dynamics observed by current satellite missions using dense ground measurements. The lack of temporal resolution in remote sensing data sets translates to a lack of understanding of glacier terminus processes and therefore limits our ability to accurately model marine-terminating glaciers.

Comparing strain rate and velocity maps derived by GPRI to other satellite datasets, it is clear that a narrow band of high stresses and high speeds occurs at the ice front that is not observable by satellite data. We calculate stresses ranging from 600 to 900 kPa near the calving margin, while satellite measurements indicate stress values that remain below 500 kPa, largely underestimating the peak stress values. This is highly problematic when relying on satellite data to model the calving dynamics of marine-terminating glaciers. Morlighem2016 uses a calving law based on the von Mises (VM) stress which has been shown to produce the best fit with observations Choi2018. In this approach, calving occurs when the tensile stress exceeds a threshold σ_{max}. In previous chapters, we use a deformation constant of 324 kPa/yr$^{1/3}$ (value for ice at -5°C, with an uncertainty of 25% (Cuffey and Paterson, 2010)) to convert the strain rates into stresses. With this selection of deformation constant, we calculate stresses ranging from 600 to 900 kPa near the calving margin, again higher than what is reported by satellite acquisitions. The low values of σ_{max} reported by satellite data would overestimate calving rates if employed in a numerical model. It will be important to ice sheet models in the future to examine glaciers as we have here to evaluate the true value of σ_{max}. Values calculated using coarse resolution velocity measurements from speckle tracking or optical tracking should be accompanied by the understanding that these results have the tendency to overestimate.

Many glaciers have been shown to be modulated by tidal height with the relationship varying by glacier. Glaciers studied in Greenland and Alaska out-of-phase relationships with tidal

height (O'Neel et al., 2001; Davis et al., 2014; Voytenko et al., 2015; Holland et al., 2016; Podrasky et al., 2014; Cassotto et al., 2018), similarly to what is observed at Kujalleq Sermeq and in opposition to what is observed at Kangilernata Sermia. In addition, non-linear responses to changes in tidal height have been noted for glaciers with floating ice shelves (Brunt et al., 2010; King et al., 2010; Makinson et al., 2012; Padman et al., 2018). Tidal effects have been seen on the bi-monthly timescale with the highest speeds at spring tide and lowest at neap tide (Gudmundsson, 2006), at Rutford Ice Stream.

The pattern of speed change due to tidal height is widespread, effecting a large portion of the glacier, across a majority of the ice front (Figs 2.3 and 3.6). Tidal height modulates the glacier up to 20-30% with speed change decreasing with distance from the front. This differs greatly from the pattern of speed change observed after the calving of grounded ice.

Calving events that remove grounded ice decrease basal resistance, increasing the glacier's ability to flow. Events that calve floating ice do not change the force balance of the glacier, and therefor cause no change in glacier flow speed. Two calving events studied here (Chapters 2 and 3) removed grounded ice and showcase this increase in speed. The speed increase is localized, not extending far from the area calved, and range from 16-31%.

Similar calving induced speed increases have been observed at other glaciers in Greenland, including Jakobshavn Isbrae (Cassotto et al., 2018) and Helheim Glacier (Holland et al., 2016). These studies, along with the 2018 study at Torsukatak Fjord (Chapter 3), are done without support of high quality bathymetry needed to determine if ice blocks were grounded before removal. In such studies, it can only be assumed that the events followed by a localized increase in ice speed removed a portion of grounded ice, changing the force balance across the glacier front. This assumption is possible when using the results of Chapter 2 as verification. At Kangilernata Sermia, MBES data had been collected up to and underneath the ice front. This high-resolution bathymetry data allowed for high resolution maps of ice thickness and therefore calculations of height above floatation with low uncertainty. Here we were able

to conclude that the only calving event that caused a localized speed increase removed a portion of grounded ice. The lack of speed up upstream of the ice front indicates that the stress coupling between the ice front and the remainder of the glacier decays quickly, within one ice thickness.

The localized speed increase persists for multiple hours to days after the calving event occurs. We suggest that the glacier speed will return to its original speed only once the ice front has replaced the removed grounded ice, on the order of 2-3 weeks time. This is comparable to the results of a similar study at Jakobshavn Isbrae (Cassotto et al., 2018). Neither study presented here extended long enough to capture the ice front return to its original position.

A relationship has been shown to exist between runoff and enhanced sliding at other marine-terminating glaciers in Greenland (Holland et al., 2016), however any such relationship was not observed in the GPRI studies presented in previous chapters. With only daily averaged runoff data available, no correlation is found with either 12-hour or 24-hour stacked GPRI derived ice speeds. In order to look into this relationship further, higher resolution runoff data would be necessary.

The multi-looked radar backscatter intensity (MLI) data (Fig. 3.4) can be used to track the motion in the fjord at the glacier front. Greenland's fjords can be highly dynamic with various circulation patterns over a short period of time. The MLI data can be used to track debris and icebergs or melange at the surface to infer horizontal surface water motion and how surface circulation can be altered. From the MLI imagery we were able to track calving events and the resulting gravity waved produced from the falling ice. These waves can change the surface circulation and effect the melange pattern and concentration in the fjord. Future projects studying fjord water dynamics could greatly benefit from GPRI data of the fjord motion at a temporal resolution of 3 minutes.

4.2 Conclusions

With the goal of improving how remote sensing is used to study the cryosphere, this project studied the processes that occur between satellite acquisitions by increasing the temporal resolution of ice speed and elevation measurements during the calving season. The application of optical and radar satellites has been transformative for mapping ice velocity in Greenland and Antarctica. GPRI studies reveal important information missing from these measurements, in particular about tidal modulation, calving events, and strain rates along the glacier front.

Presented here are the first sub-hourly observations of speed and elevation at Kangilernata Sermia, Kujalleq Sermeq, and Avannarleq Sermeq collected using GPRI. We find that both Kangilernata Sermia and Kujalleq Sermeq are modulated by the tides and experience strong velocity fluctuations of 15-20% that effect the glaciers far inland. This differs from the pattern of speed change observed when full-thickness grounded ice is removed from the ice front, which is limited to the area around the zone of detachment. When calving removed grounded ice, this localized change in speed persists for multiple days. Removal of floating ice causes no change in glacier activity. Using GPRI we are able to detect strain rates and stresses over the entire ice front, which are often not observable or over-smoothed using typical speckle-tracking methods. We detect strain rates and stressed along the ice fronts to be 2-3 times larger than reported using satellite measurements, advancing our understanding of variables important in the modeling the break up of ice into icebergs. These findings reinforce the need to track ice motion using the interferometric phase at the pixel level instead of speckle tracking. In order to do so, satellite data must be acquired at much shorter time scale, and typically sub-daily.

This work aims improve the use of remote sensing techniques on marine-terminating glaciers in the future and therefore the regional climate models that use these observations to predict

the state of our climate. With emphasis on how short-term perturbations effect glacier speed, the knowledge gained with this study can be applied to future airborne and space missions to help plan and interpret remote sensing observations. This research will be instrumental in determining what best temporal resolution SAR systems should achieve to observe marine-terminating glacier dynamics.

4.3 Outlook

This work showcases the unprecedented level of detail that can be observed at glacier calving margins when acquiring data at the sub-hourly time scale. The importance of this work spans governmental agencies planning future space missions to the ability of an individual person to buy beach-front property insurance. The knowledge gained from observing glaciers at sub-hourly time scales can be used to plain future space missions and used to improve predictions of future sea level rise in ice sheet models.

Governmental agencies should use the results described here to plan for future satellite data acquisitions, recognizing the importance of limiting the time between repeat passes to increase coverage at the ice front. Studies of short-time scale glacier dynamics,such as those presented here, can be used to design the next generation of InSAR missions. Here we shed light on what can be gained from high temporal resolution and what is missed by current missions with large repeat pass cycling. We have provided data that will go into future decision making about InSAR missions. We have shown that interferometric phase can be used up to the ice front when collected with a temporal resolution on the order of hours. This is a great improvement from the currently used speckle tracking method that does not provide data within a few hundred meters of the ice front. Future studies of grounding lines and grounding line migration could benefit from using a GPRI or similar ground-based SAR instrument to collect high resolution data throughout the day.

These observations and results can also be incorporated into future ice sheet models to improve predictions of ice front dynamics. Ice sheet models are lacking observations and understanding of how marine terminating glaciers will react to changes in climate warming. The results from this study and others of this scale can be used to improve future ice sheet models and increase the accuracy of future sea level rise predictions.

Future GPRI campaigns must be coupled with a high resolution bathymetric understanding of the fjord up to and underneath the ice front in order to conclude on the importance of calving grounded vs. floating ice. Without high resolution bathymetry data, it is impossible to determine if the iceberg was grounded or floating prior to detachment. Future observations and results of calving events such as those from Kangilernata Sermia, presented here (Chapter 2), are essential in increasing understanding of calving dynamics at marine-terminating glaciers.

Field campaigns and analysis of GPRI data at marine terminating ice fronts should continue, with the goal of observing glaciers with varying conditions. Furthering understanding of short-time scale dynamics at ice fronts with differing characteristics will be of continued importance as glaciers and ice sheets continue to be the leading contributors to sea level rise.

4.4 Acknowledgements

This work was performed in the Department of Earth System Science, University of California Irvine, at Caltech's Jet Propulsion Laboratory, and at the University of Alaska, Fairbanks, under a contract with the National Aeronautics and Space Administration grants #NNX17AI02G and 80NSSC18M0083, and Ocean Melting Greenland Award #1528152. Bathymetry data are available publicly at Caltech's Jet Propulsion Laboratory (omg.jpl.nasa.gov). TanDEM-X SAR data were provided by DLR (German Space Agency) through proposal

XTI_GLAC0508. Satellite ice velocity data have been deposited in University of California, Irvine Dryad (UCI Dryad) (DOIs: 10.7280/ D1MM37, 10.7280/D1GW91, 10.7280/D1595V, 10.7280/D1595V, and 10.7280/D11H3X) as well as GPRI ice velocity data and average DEM (DOIs: 10.7280/D1R085).

Bibliography

OMG 2016. Omg mission: Bathymetry (sea floor depth) data from the ship-based bathymetry survey. ver. 0.1 (tech. rep.). ca, usa. 2016.

J. M. Amundson, M. Truffer, M. P. Lüthi, M. Fahnestock, M. West, and R. J. Motyka. Glacier, fjord, and seismic response to recent large calving events, Jakobshavn Isbræ, Greenland. *Geophysical Research Letters*, 35(22):L22501, 2008. ISSN 0094-8276. doi: 10.1029/2008GL035281.

L. An, E. Rignot, J. Mouginot, and R. Millan. A Century of Stability of Avannarleq and Kujalleq Glaciers, West Greenland, Explained Using High-Resolution Airborne Gravity and Other Data. *Geophysical Research Letters*, 45(7):3156–3163, 2018. ISSN 0094-8276, 1944-8007. doi: 10.1002/2018GL077204.

Anker Weidick. Observations on some Holocene glacier fluctuations in West Greenland. *Reitzel*, 1968.

Douglas I. Benn, Charles R. Warren, and Ruth H. Mottram. Calving processes and the dynamics of calving glaciers. *Earth-Science Reviews*, 82(3-4):143–179, 2007. ISSN 00128252. doi: 10.1016/j.earscirev.2007.02.002.

Kelly M. Brunt, Matt A. King, Helen Amanda Fricker, and Douglas R. MacAyeal. Flow of the Ross Ice Shelf, Antarctica, is modulated by the ocean tide. *Journal of Glaciology*, 56 (195):157–161, 2010. ISSN 0022-1430, 1727-5652. doi: 10.3189/002214310791190875.

Ryan Cassotto, Mark Fahnestock, Jason M. Amundson, Martin Truffer, and Ian Joughin. Seasonal and interannual variations in ice melange and its impact on terminus stability, Jakobshavn Isbr&aelig, Greenland. *Journal of Glaciology*, 61(225):76–88, 2015. ISSN 00221430, 17275652. doi: 10.3189/2015JoG13J235.

Ryan Cassotto, Mark Fahnestock, Jason M. Amundson, Martin Truffer, Margaret S. Boettcher, Santiago De La Peña, and Ian Howat. Non-linear glacier response to calving events, Jakobshavn Isbræ, Greenland. *Journal of Glaciology*, pages 1–16, 2018. ISSN 0022-1430, 1727-5652. doi: 10.1017/jog.2018.90.

Youngmin Choi, Mathieu Morlighem, Michael Wood, and Johannes H. Bondzio. Comparison of four calving laws to model Greenland outlet glaciers. *The Cryosphere*, 12(12):3735–3746, 2018. ISSN 1994-0424. doi: 10.5194/tc-12-3735-2018.

F Covello, F. Battazza, A. Coletta, E. Lopinto, C. Fiorentino, L. Pietranera, G. Valentini, and S. Zoffoli. COSMO-SkyMed an existing opportunity for observing the Earth. *Journal of Geodynamics*, 49(3-4):171–180, 2010. ISSN 02643707. doi: 10.1016/j.jog.2010.01.001.

K.M. Cuffey and W.S.B. Paterson. The physics of glaciers, fourth edition. *Elseview*, page 693 pp., 2010.

J.L. Davis, J. De Juan, M. Nettles, P. Elosegui, and M.L. Andersen. Evidence for non-tidal diurnal velocity variations of Helheim Glacier, East Greenland. *Journal of Glaciology*, 60 (224):1169–1180, 2014. ISSN 0022-1430, 1727-5652. doi: 10.3189/2014JoG13J230.

Robert M. DeConto and David Pollard. Contribution of Antarctica to past and future sea-level rise. *Nature*, 531(7596):591–597, 2016. ISSN 0028-0836, 1476-4687. doi: 10.1038/nature17145.

Richard M. Goldstein, Howard A. Zebker, and Charles L. Werner. Satellite radar interferometry: Two-dimensional phase unwrapping. *Radio Science*, 23(4):713–720, 1988. ISSN 00486604. doi: 10.1029/RS023i004p00713.

G. Hilmar Gudmundsson. Fortnightly variations in the flow velocity of Rutford Ice Stream, West Antarctica. *Nature*, 444(7122):1063–1064, 2006. ISSN 0028-0836, 1476-4687. doi: 10.1038/nature05430.

G. Hilmar Gudmundsson. Tides and the flow of rutford ice stream, west antarctica. *J. Geophys. Res.*, 112:F04007, 2007.

David M. Holland, Denis Voytenko, Timothy Dixon, Jeffrey Mei, Byron Parizek, Irena Vaňková, Ryan Walker, Jacob Walter, Keith Nicholls, and Denise Holland. An intensive observation of calving at helheim glacier, east greenland. *Oceanography*, 29(4):46–61, 2016. doi: 10.5670/oceanog.2016.98.

I. M. Howat, A. Negrete, and B. E. Smith. The Greenland Ice Mapping Project (GIMP) land classification and surface elevation data sets. *The Cryosphere*, 8(4):1509–1518, August 2014. ISSN 1994-0424. doi: 10.5194/tc-8-1509-2014. URL `https://www.the-cryosphere.net/8/1509/2014/`.

Adrian Jenkins and Stan Jacobs. Circulation and melting beneath George VI Ice Shelf, Antarctica. *Journal of Geophysical Research*, 113(C4):C04013, 2008. ISSN 0148-0227. doi: 10.1029/2007JC004449. URL `http://doi.wiley.com/10.1029/2007JC004449`.

Ian Joughin, Ben E. Smith, Ian M. Howat, Dana Floricioiu, Richard B. Alley, Martin Truffer, and Mark Fahnestock. Seasonal to decadal scale variations in the surface velocity of Jakobshavn Isbrae, Greenland: Observation and model-based analysis: JAKOBSHAVN ISBRAE, OBSERVATION/ANALYSIS. *Journal of Geophysical Research: Earth Surface*, 117(F2):n/a–n/a, 2012. ISSN 01480227. doi: 10.1029/2011JF002110.

Matt A. King, Tavi Murray, and Andy M. Smith. Non-linear responses of Rutford Ice Stream, Antarctica, to semi-diurnal and diurnal tidal forcing. *Journal of Glaciology*, 56 (195):167–176, 2010. ISSN 0022-1430, 1727-5652. doi: 10.3189/002214310791190848.

R. Kwok and M.A. Fahnestock. Ice sheet motion and topography from radar interferometry. *IEEE Transactions on Geoscience and Remote Sensing*, 34(1):189–200, 1996. ISSN 01962892. doi: 10.1109/36.481903.

Keith Makinson, Matt A. King, Keith W. Nicholls, and G. Hilmar Gudmundsson. Diurnal and semidiurnal tide-induced lateral movement of Ronne Ice Shelf, Antarctica: TIDAL MOVEMENT OF RONNE ICE SHELF. *Geophysical Research Letters*, 39(10), 2012. ISSN 00948276. doi: 10.1029/2012GL051636.

Daniel McGrath, William Colgan, Konrad Steffen, Phillip Lauffenburger, and James Balog. Assessing the summer water budget of a moulin basin in the Sermeq Avannarleq ablation region, Greenland ice sheet. *Journal of Glaciology*, 57(205):954–964, 2011. ISSN 00221430, 17275652. doi: 10.3189/002214311798043735. McGrath2011.

Pietro Milillo, Eric Rignot, Jeremie Mouginot, Bernd Scheuchl, Mathieu Morlighem, Xin Li, and Jacqueline T. Salzer. On the Short-term Grounding Zone Dynamics of Pine Island Glacier, West Antarctica, Observed With COSMO-SkyMed Interferometric Data: PIG Grounding Line Dynamics. *Geophysical Research Letters*, 44(20):10,436–10,444, 2017. ISSN 00948276. doi: 10.1002/2017GL074320.

M. Morlighem, J. Bondzio, H. Seroussi, E. Rignot, E. Larour, A. Humbert, and S. Rebuffi. Modeling of Store Gletscher's calving dynamics, West Greenland, in response to ocean thermal forcing. *Geophysical Research Letters*, 43(6):2659–2666, 2016. ISSN 0094-8276, 1944-8007. doi: 10.1002/2016GL067695.

Roman J. Motyka, Lewis Hunter, Keith A. Echelmeyer, and Cathy Connor. Submarine melting at the terminus of a temperate tidewater glacier, LeConte Glacier, Alaska, U.S.A. *Annals of Glaciology*, 36:57–65, 2003. ISSN 0260-3055, 1727-5644.

Jeremie Mouginot, Eric Rignot, Bernd Scheuchl, and Romain Millan. Comprehensive annual ice sheet velocity mapping using landsat-8, sentinel-1, and radarsat-2 data. *Remote Sensing*, 9(4):364, 2017. ISSN 2072-4292. doi: 10.3390/rs9040364.

Jérémie Mouginot, Eric Rignot, Anders A. Bjørk, Michiel van den Broeke, Romain Millan, Mathieu Morlighem, Brice Noël, Bernd Scheuchl, and Michael Wood. Forty-six years of Greenland Ice Sheet mass balance from 1972 to 2018. *Proceedings of the National Academy of Sciences*, page 201904242, 2019. ISSN 0027-8424, 1091-6490. doi: 10.1073/pnas.1904242116.

M. Nettles, T. B. Larsen, P. Elósegui, G. S. Hamilton, L. A. Stearns, A. P. Ahlstrøm, J. L. Davis, M. L. Andersen, J. de Juan, S. A. Khan, L. Stenseng, G. Ekström, and R. Forsberg. Step-wise changes in glacier flow speed coincide with calving and glacial earthquakes at Helheim Glacier, Greenland. *Geophysical Research Letters*, 35(24):L24503, 2008. ISSN 0094-8276. doi: 10.1029/2008GL036127.

B Noël, WJ Van De Berg, E Van Meijgaard, P Kuipers Munneke, R Van De Wal, and MR Van Den Broeke. Evaluation of the updated regional climate model RACMO2. 3:

summer snowfall impact on the Greenland Ice Sheet. *The Cryosphere*, 9(5):1831–1844, 2015.

S. O'Neel, K. A. Echelmeyer, and R. J. Motyka. Short-term flow dynamics of a retreating tidewater glacier: LeConte Glacier, Alaska, U.S.A. *Journal of Glaciology*, 47(159):567–578, 2001. ISSN 0022-1430, 1727-5652. doi: 10.3189/172756501781831855.

Laurie Padman, Matthew R. Siegfried, and Helen A. Fricker. Ocean Tide Influences on the Antarctic and Greenland Ice Sheets: Tide Influences on Ice Sheets. *Reviews of Geophysics*, 56(1):142–184, 2018. ISSN 87551209. doi: 10.1002/2016RG000546.

David Podrasky, Martin Truffer, Martin Lüthi, and Mark Fahnestock. Quantifying velocity response to ocean tides and calving near the terminus of Jakobshavn Isbræ, Greenland. *Journal of Glaciology*, 60(222):609–621, 2014. ISSN 0022-1430, 1727-5652. doi: 10.3189/2014JoG13J130.

Claire Porter, Paul Morin, Ian Howat, Myoung-Jon Noh, Brian Bates, Kenneth Peterman, Scott Keesey, Judith Schlenk, Matthew; Gardiner, Karen Tomko, Michael Willis, Cole Kelleher, Michael Cloutier, Eric Husby, Steven Foga, Hitomi Nakamura, Melisa Platson, Jr. Wethington, Michael, Cathleen Williamson, Gregory Bauer, Jeremy Enos, Galen Arnold, William Kramer, Peter Becker, Abhijit Doshi, Cristelle D'Souza, Pat Cummens, Fabien Laurier, and Mikkel Bojesen. Arcticdem. *Harvard Dataverse*, V1, 2018. doi: https://doi.org/10.7910/DVN/OHHUKH.

Patrick Riesen, Tazio Strozzi, Andreas Bauder, Andreas Wiesmann, and Martin Funk. Short-term surface ice motion variations measured with a ground-based portable real aperture radar interferometer. *Journal of Glaciology*, 57(201):53–60, 2011.

E. Rignot and J. Mouginot. Ice flow in Greenland for the International Polar Year 2008-2009: ICE FLOW GREENLAND 2009. *Geophysical Research Letters*, 39(11):n/a–n/a, 2012. ISSN 00948276. doi: 10.1029/2012GL051634.

E. Rignot, J. E. Box, E. Burgess, and E. Hanna. Mass balance of the Greenland ice sheet from 1958 to 2007. *Geophysical Research Letters*, 35(20), 2008. ISSN 0094-8276. doi: 10.1029/2008GL035417.

E. Rignot, Y. Xu, D. Menemenlis, J. Mouginot, B. Scheuchl, X. Li, M. Morlighem, H. Seroussi, M. van den Broeke, I. Fenty, C. Cai, L. An, and B. de Fleurian. Modeling of ocean-induced ice melt rates of five west Greenland glaciers over the past two decades: MODELING OF GLACIER MELT IN GREENLAND. *Geophysical Research Letters*, 43(12):6374–6382, 2016. ISSN 00948276. doi: 10.1002/2016GL068784.

Eric Rignot, Michele Koppes, and Isabella Velicogna. Rapid submarine melting of the calving faces of West Greenland glaciers. *Nature Geoscience*, 3(3):187–191, March 2010. ISSN 1752-0894, 1752-0908. doi: 10.1038/ngeo765. URL `http://www.nature.com/articles/ngeo765`.

Eric Rignot, Ian Fenty, Yun Xu, Cilan Cai, and Chris Kemp. Undercutting of marine-terminating glaciers in West Greenland: GLACIER UNDERCUTTING BY OCEAN WATERS. *Geophysical Research Letters*, 42(14):5909–5917, 2015. ISSN 00948276. doi: 10.1002/2015GL064236.

Robert Massom, Dan Lubin. *Polar Remote Sensing*, volume 2. Springer, 2006. ISBN 3-540-26101-X.

Andrew Shepherd, Alun Hubbard, Peter Nienow, Matt King, Malcolm McMillan, and Ian Joughin. Greenland ice sheet motion coupled with daily melting in late summer. *Geophysical Research Letters*, 36(1), 2009. ISSN 0094-8276. doi: 10.1029/2008GL035758.

Fiammetta Straneo, Gordon S. Hamilton, David A. Sutherland, Leigh A. Stearns, Fraser Davidson, Mike O. Hammill, Garry B. Stenson, and Aqqalu Rosing-Asvid. Rapid circulation of warm subtropical waters in a major glacial fjord in East Greenland. *Nature Geoscience*, 3(3):182–186, 2010. ISSN 1752-0894, 1752-0908. doi: 10.1038/ngeo764. URL `http://www.nature.com/articles/ngeo764`.

Shin Sugiyama and G. Hilmar Gudmundsson. Short-term variations in glacier flow controlled by subglacial water pressure at Lauteraargletscher, Bernese Alps, Switzerland. *Journal of Glaciology*, 50(170):353–362, 2004.

Denis Voytenko, Alon Stern, David M. Holland, Timothy H. Dixon, Knut Christianson, and Ryan T. Walker. Tidally driven ice speed variation at helheim glacier, greenland, observed with terrestrial radar interferometry. *Journal of Glaciology*, 61(226):301–308, 2015.

Charles Werner, Tazio Strozzi, Andreas Wiesmann, and Urs Wegmuller. A real-aperture radar for ground-based differential interferometry. 3:III–210, 2008.

M. Wood, E. Rignot, I. Fenty, D. Menemenlis, R. Millan, M. Morlighem, J. Mouginot, and H. Seroussi. Ocean-induced melt triggers glacier retreat in northwest greenland. *Geophysical Research Letters*, 45(16):8334–8342, 2018. ISSN 0094-8276, 1944-8007. doi: 10.1029/2018GL078024.

Surui Xie, Timothy H. Dixon, Denis Voytenko, Fanghui Deng, and David M. Holland. Grounding line migration through the calving season at Jakobshavn Isbræ, Greenland, observed with terrestrial radar interferometry. *The Cryosphere*, 12(4):1387–1400, 2018. ISSN 1994-0424. doi: 10.5194/tc-12-1387-2018.

Surui Xie, Timothy H. Dixon, David M. Holland, Denis Voytenko, and Irena Vaňková. Rapid iceberg calving following removal of tightly packed pro-glacial mélange. *Nature Communications*, 10(1):3250, 2019. ISSN 2041-1723. doi: 10.1038/s41467-019-10908-4.